Chemical Geology 540 (2020) 119482

Contents lists available at ScienceDirect

Chemical Geology

journal homepage: www.elsevier.com/locate/chemgeo

Magnesium isotope analysis of olivine and pyroxene by SIMS: Evaluation of matrix effects

Kohei Fukuda[a,*], Brian L. Beard[a], Daniel R. Dunlap[b], Michael J. Spicuzza[a], John H. Fournelle[a], Meenakshi Wadhwa[b], Noriko T. Kita[a]

[a] Department of Geoscience, University of Wisconsin-Madison, Madison, WI 53706, USA
[b] School of Earth and Space Exploration, Arizona State University, Tempe, AZ 85287, USA

ARTICLE INFO

Editor: Balz Kamber

Keywords:
Secondary ion mass spectrometry
Inductively coupled plasma mass spectrometry
Magnesium isotopes
Matrix effects
Olivine and pyroxene

ABSTRACT

The performance of multi-collector secondary ion mass spectrometry (MC-SIMS) for Mg isotope ratio analysis was evaluated using 17 olivine and 5 pyroxene reference materials (RMs). The Mg isotope composition of these RMs was accurately and precisely determined by multi-collector inductively coupled plasma mass spectrometry (MC-ICP-MS), and these measured isotope ratios were used to evaluate SIMS instrumental mass bias as a function of the forsterite (Fo) content of olivine. The magnitude of the Mg isotope matrix effects were ~3‰ in δ^{25}Mg, and are a complex function of olivine Fo content, that ranged from $Fo_{59.3}$ to Fo_{100}. In addition to these Mg isotope matrix effects, Si^+ ion yields and Mg^+/Si^+ ion ratios varied as a complex function of the Fo content of the olivine RMs. For example, Si^+ ion yields varied by ~33%. Based on the observations, we propose instrumental bias correction procedures for SIMS Mg isotope analysis of olivine using a combination of Mg^+/Si^+ ratios and Fo content of olivine. Using this correction method, the accuracy of δ^{25}Mg analyses is 0.3‰, except for analysis of olivine with $Fo_{86–88}$ where instrumental biases and Mg^+/Si^+ ratios change dramatically with Fo content, making it more difficult to assess the accuracy of Mg isotope ratio measurements by SIMS over this narrow range of Fo content.

Five pyroxene RMs (3 orthopyroxenes and 2 clinopyroxenes) show smaller ranges of instrumental bias (~1.4‰ in δ^{25}Mg) as compared to the olivine RMs. The instrumental bias for the 3 orthopyroxene RMs do not define a linear relationship with respect to enstatite (En) content, that ranged from $En_{85.5–96.3}$. The clinopyroxene RMs have similar En and wollastonite (Wo) contents but have δ^{25}Mg values that differ by 0.5‰ relative to their δ^{25}Mg values determined by MC-ICP-MS. These results indicate that additional factors (e.g., minor element abundances) likely contribute to SIMS instrumental mass fractionation. In order to better correct for these SIMS matrix effects, additional pyroxene RMs with various chemical compositions and known Mg isotope ratios are needed.

1. Introduction

Magnesium is a major rock-forming element and seventh most abundant element in the Solar System. Magnesium has three naturally occurring stable isotopes (^{24}Mg, ^{25}Mg, and ^{26}Mg) allowing us to study mass-dependent and mass-independent isotope fractionation induced by natural processes. Three analytical approaches are commonly taken to obtain high precision Mg isotope data: solution nebulization multi-collector inductively coupled plasma mass spectrometry (SN-MC-ICP-MS), laser ablation MC-ICP-MS (LA-MC-ICP-MS), and multi-collector secondary ion mass spectrometry (MC-SIMS). Among them, SN-MC-ICP-MS analyses of Mg isotopes are the most reliable. This method entails dissolution of the sample followed by quantitative separation of Mg from all other cations by ion exchange chromatography and Mg isotope ratio analysis using a standard bracketing technique (e.g., Galy et al., 2001; Teng et al., 2010). SN-MC-ICP-MS has been applied to solve important geochemical and cosmochemical questions, such as mantle metasomatism (e.g., Xiao et al., 2013; Hu et al., 2016a; Teng, 2017 and references therein), continental weathering (e.g., Tipper et al., 2006; Pogge von Strandmann et al., 2008), distribution of Mg isotopes in the Earth and early solar system (e.g., Handler et al., 2009; Teng et al., 2010; Schiller et al., 2010; Bourdon et al., 2010; Sedaghatpour and Teng, 2016; Van Kooten et al., 2016; Olsen et al., 2016), radiogenic ^{26}Mg excesses produced by the decay of short-lived ^{26}Al (e.g., Jacobsen

* Corresponding author.
E-mail address: kfukuda2@wisc.edu (K. Fukuda).

https://doi.org/10.1016/j.chemgeo.2020.119482
Received 4 October 2019; Received in revised form 25 January 2020; Accepted 27 January 2020
Available online 31 January 2020

et al., 2008; Larsen et al., 2011; Wasserburg et al., 2012), and condensation and evaporation processes in the solar nebula (e.g., Richter et al., 2007; Davis et al., 2015). Meteoritic samples, such as Ca, Al-rich inclusions (CAIs), show micro-scale variations in radiogenic ^{26}Mg and/or the degree of mass-dependent fractionation, and these Mg isotope composition have been determined by both LA-MC-ICP-MS and MC-SIMS at the 5–100 μm spatial resolutions (e.g., Young et al., 2002; Kita et al., 2012; MacPherson et al., 2012, 2017; Bullock et al., 2013; Kawasaki et al., 2015, 2017, 2018, 2019; Ushikubo et al., 2017; Mendybaev et al., 2017; Williams et al., 2017).

Isotope ratios measured by the above three mass spectrometric techniques are inherently different from the absolute Mg isotope ratios of samples due to instrumental mass fractionation (IMF) (e.g., Eiler et al., 1997; Albarède et al., 2004; Horn and von Blanckenburg, 2007). Typically, IMF is corrected by normalization to a standard run under the same conditions as the sample. A bias in this IMF correction can be produced if the sample and standard are not identical in composition, and this bias is often referred to as a matrix or non-spectral interference (e.g., Albarède and Beard, 2004). For SN-MC-ICP-MS, matrix effects are eliminated by purifying samples by ion exchange chromatography and matching the Mg concentration of samples and standards when doing isotope ratio measurements. In contrast, for in-situ techniques, this purification step is not possible and thus LA-ICP-MS and SIMS analysis can be strongly affected by sample matrix. Chaussidon et al. (2017) argued that matrix correction is typically much larger for SIMS than LA-ICP-MS. Thus, matrix-matched standards are always required to obtain accurate Mg isotope data using SIMS techniques. For LA-ICP-MS matrix effects can be minimized or eliminated by use of lasers with ultra-short pulse widths and by loading the plasma with small amounts of water that is co-aspirated into the instrument with the ablated material (Oeser et al., 2014).

In spite of matrix effects that compromise the accuracy of in-situ Mg isotope analyses, the SIMS technique has been successfully used to identify large mass-dependent isotope fractionations (>10‰/amu) in Mg isotopes that have been observed in CAIs with Fractionation and Unidentified Nuclear (FUN) effects (e.g., Krot et al., 2014 and reference therein; Park et al., 2017 and reference therein). Magnesium isotope ratios of FUN CAIs are positively fractionated up to 45‰/amu (e.g., Park et al., 2017), suggesting that FUN CAIs experienced intense evaporation events under near vacuum conditions (Mendybaev et al., 2013, 2017). Technical improvements on the MC-SIMS Mg isotope analysis over the last decade (e.g., Kita et al., 2012; Luu et al., 2013) allow us to investigate mass-dependent fractionation effects smaller than 10‰/amu in CAIs. For example, Mg isotope zoning of melilite in coarse grained CAIs was successfully determined at sub‰ level by MC-SIMS by correcting the SIMS matrix effects of δ^{25}Mg in melilite solid-solution that changes linearly with Åkermanite contents (Kita et al., 2012; Bullock et al., 2013).

Ushikubo et al. (2013) conducted high precision SIMS Mg isotope analysis of multiple phases in chondrules and calibrated instrumental bias on olivine based on a linear correlation between instrumental bias and Fo content (Fo = [Mg]/[Mg + Fe] molar %) observed in 4 olivine standards (Fo_{59} to Fo_{100}). Olivine in chondrules tends to show positively fractionated Mg isotope ratios (up to 2.3‰/amu) relative to coexisting phases (pyroxene and plagioclase). Based on these observations, Ushikubo et al. (2013) suggested that chondrule melting occurred in an open system. Recently, however, Chaussidon et al. (2017) evaluated matrix effects on Mg isotope analyses of olivine and silicate glasses by SIMS and found complex IMF in olivine as a function of Fo content. Consequently, Mg isotope ratios of olivine in chondrules reported in Ushikubo et al. (2013) might not be accurate due to unrecognized matrix effects. Furthermore, Ushikubo et al. (2013) assumed that the Mg isotope composition of these four olivine standards (including one synthetic olivine) is the same as the Earth's mantle (−0.13‰ relative to the DSM-3 standard; Teng et al., 2010). This assumption, at least for the synthetic olivine standard, may not be valid because Mg isotope compositions of starting materials do not need to be the same as the Earth's mantle and synthetic processes may induce mass-dependent fractionation (e.g., Kita et al., 2012). In order to evaluate mass-dependent fractionation effects in olivine and pyroxene from extraterrestrial materials, it is important to develop suitable reference materials so that the matrix effects associated with SIMS analysis can be fully evaluated.

In this paper, we evaluate matrix effects on SIMS Mg isotope analysis of olivine and pyroxene. We prepared 17 olivine and 5 pyroxene reference materials (RMs) with various chemical compositions. The Mg isotope ratios of individual RMs were determined relative to the DSM-3 scale by either SN-MC-ICP-MS or by LA-MC-ICP-MS techniques, depending on the quantity of available RM and the degree to which high purity mineral separates could be produced. RMs with limited amounts of material, or which were difficult to separate, were analyzed by LA-MC-ICP-MS. These RMs were then subjected to MC-SIMS three Mg isotope ratio measurements. Moreover, major- and minor-element analyses of these olivine RMs were also performed by SIMS and electron microprobe in order to evaluate the relationship between instrumental biases and ionization efficiencies of each element as compared to the chemical composition of the olivine RMs that were determined by electron microprobe analysis. Our goal is to evaluate the applicability of high precision and high spatial resolution SIMS Mg isotope analysis. This work is critical to allow one to assess the accuracy of Mg isotope ratio analysis of extraterrestrial olivine and pyroxene samples, such as those in chondrule and amoeboid olivine aggregate from primitive meteorites, as well as small and precious particles obtained by sample return missions (e.g., *Stardust*, *Hayabusa2*, and *OSIRIS-REx*).

2. Sample preparation

Seventeen olivine (11 terrestrial, 5 meteoritic, and one synthetic) and 5 terrestrial pyroxene RMs were used in this study. Four olivine (SC-Ol, HN-Ol, IG-Ol, and OR-Ol) and all pyroxene RMs in the suite of standards have been used as SIMS calibration standards for oxygen isotope analyses (Kita et al., 2010). Mg isotope ratios of 3 olivine RMs (CL09-08, 19, and 33-Ol) were previously reported in the literature (Xiao et al., 2013). Importantly, the RMs considered in this study also include 5 meteoritic olivine samples. Meteoritic olivine has distinct chemical compositions (in terms of both Fo contents and minor-element abundances), as compared to terrestrial olivine samples. A list of the RMs is reported in Table 1. Eleven olivine and all pyroxene RMs were either taken from mineral separates or handpicked from sieved grain-size fractions that had a range of grain sizes from 100 μm–1000 μm. Aliquots of 5 olivine RMs (KN-Ol, CL09-19-Ol, CL09-08-Ol, CL09-33-Ol, and WN-Ol) were separated from host rocks and meteorites in this study. Olivine grains in Winona meteorite (WN-Ol) were small (~100 μm) and intermixed with metals, so several ~1 mm sized chips of Winona meteorites were mounted in epoxy resin and polished; chips containing olivine-rich areas were then extracted from the epoxy resin and used for this study. The RM, N7325-Ol, is from olivine grains from an ungrouped achondrite (NWA 7325), that has Mg-rich olivine ($Fo_{97.4}$). This RM was obtained from a polished thick section studied by Goodrich et al. (2017). Detail descriptions of each RM, and procedures used for separating olivine grains are summarized in Appendix EA1. Except the WN-Ol and N7325-Ol, 1 to 42 grains (typically 20 grains) of each RM were handpicked under a binocular microscope and mounted in 25 mm diameter epoxy disks for electron microprobe, LA-MC-ICP-MS, and SIMS analysis. Among them, limited numbers of grains (one or two grains) were handpicked for SC-Ol and HN-Ol because they have larger grain sizes (~1 mm) and are known to be homogeneous in their Mg isotope ratios (e.g., Ushikubo et al., 2013). In addition, only two grains of A77257-Ol were handpicked and used for this study because we only have 3 olivine grains of this RM. All grains and Winona chips were placed within a radius of 7 mm from the geometrical center of the mount to minimize instrumental mass fractionation effects due to

Table 1
List of olivine and pyroxene RMs used in this study.

Sample name	Fo or En content[a]	Provenance/meteorite name (type)	Rock type
Olivine			
OR-Ol	59.3	Orikabe plutonic complex, Japan	Gabbro
FJ-Ol	73.4	Mount Fuji, Japan	Gabbro
KN-Ol	78.0	Kenna (Ureilite)	Meteorite
CL09-19-Ol	79.4	Beiyan, China	Peridotite
CL09-08-Ol	80.5	Beiyan, China	Peridotite
SW-Ol	81.8	Springwater (Pallasite)	Meteorite
A77257-Ol	85.7	ALHA77257 (Ureilite)	Meteorite
CL09-33-Ol	86.6	Beiyan, China	Peridotite
SC-Ol	88.8	San Carlos, USA	Peridotite
UWOL-1	89.2	Kilbourne Hole, USA	Peridotite
IG-Ol	89.6	Ichinome-gata, Japan	Peridotite
HaK-Ol	91.9	Harrat al Kishb, Saudi Arabia	Peridotite
WK-Ol	94.3	Barberton, South Africa	Komatiite
WN-Ol	95.5	Winona (Winonaite)	Meteorite
N7325-Ol	97.4	NWA 7325 (Ungrouped achondrite)	Meteorite
SK-Ol	99.8	Isle of Skye, Scotland	Marble
HN-Ol	100.0	Synthetic forsterite	
Pyroxene			
95AK-6 Di	48.6	Adirondack Mt., USA	Marble
IG-Cpx	48.6	Ichinome-gata, Japan	Peridotite
JE En	85.5	Unknown	Unknown
IG-Opx	88.9	Ichinome-gata, Japan	Peridotite
Sp79-11 En	96.3	Adirondack Mt., USA	Enstatite

[a] Molar % of forsterite or enstatite end-members based on EPMA analyses performed in this study.

sample geometry and topography (Kita et al., 2009; Peres et al., 2013). San Carlos olivine (hereafter, SC-Ol) grains were placed near the center of each mount and these grains were used as a running standard during LA-MC-ICP-MS and SIMS analysis (the NWA 7325 thick section was originally mounted with a grain of SC-Ol). All grain mounts of olivine and pyroxene RMs and the NWA 7325 thick section were coated with carbon (20 nm thickness) for electron microprobe and SIMS analyses.

3. Experimental methods

3.1. Electron microprobe analysis

Olivine RMs were measured by electron probe micro analyzer (EPMA) in two sessions. The first session (August 2018) considered the three major and two minor element oxide (MgO, SiO_2, CaO, MnO, and FeO) concentrations of 17 olivine RMs using a Cameca SXFive FE electron microprobe at the University of Wisconsin-Madison. Analyses were performed with an accelerating voltage of 15 kV and a beam current of 20 nA, with a 3 μm diameter beam. Counting time for the peak was 10 s. Backgrounds were determined using the mean atomic number procedure (Donovan and Tingle, 1996). The following standards were used for olivine analyses: synthetic forsterite (Mg, Si), NMNH 122142 Kakanui augite (Ca), synthetic FeO (Fe), and synthetic Mn_2SiO_4 (Mn). The probe for EPMA™ (PFE) software was used for data reduction. Calculated detection limits (99% confidence) for the measured oxides listed above were 0.01, 0.02, 0.02, 0.06, and 0.04 wt%, respectively.

A second session (January 2019) for olivines added Cr_2O_3 and NiO to the list of elements, with the same column conditions. Here off peak backgrounds were acquired, with 10 s counts on the background and 10 s on the peaks. The same standards were used as above, with the addition of synthetic Cr_2O_3 for Cr and synthetic Ni_2SiO_4 for Ni. Detection limits (wt%) were: MgO-0.02, SiO_2-0.03, CaO-0.02, Cr_2O_3-0.07, MnO-0.07, FeO-0.06 and NiO-0.08.

Major and minor element oxide (Na_2O, MgO, Al_2O_3, SiO_2, CaO, TiO_2, Cr_2O_3, MnO, and FeO) concentrations of 5 pyroxene RMs were obtained with the SXFive FE electron microprobe under the same column condition for olivine analyses. Off peak backgrounds were acquired, with 10 s background and 10 s peak counting time. The following standards were used for analyses: Burma jadeite (Na), NMNH 122142 Kakanui augite (Mg, Ca), Grass Valley anorthite (Al), synthetic enstatite (Mg, Si), synthetic TiO_2 (Ti), synthetic Cr_2O_3 (Cr), synthetic Mn_2SiO_4 (Mn) and synthetic FeO (Fe). Calculated detection limits for the measured oxides in wt% were Na_2O-0.02, MgO-0.02, Al_2O_3-0.03, SiO_2-0.03, CaO-0.02, TiO_2-0.05, Cr_2O_3-0.06, MnO-0.05, and FeO-0.06 wt%. In order to evaluate grain-scale homogeneity of each of olivine and pyroxene RMs, 10–20 or 5–8 grains were typically analyzed for each of the olivine or pyroxene RMs, respectively, and individual grains were analyzed by 5 times.

In the following, Mg contents in olivine and pyroxene RMs are expressed as a Fo (=Mg/[Mg + Fe] molar %) and an En (=Mg/[Mg + Fe + Ca] molar %) contents, respectively. Likewise, Ca content in pyroxene RMs is expressed as a Wo (= Ca/[Mg + Fe + Ca] molar %) content. The Fo, En, and Wo contents were calculated by considering total iron as ferrous iron.

3.2. Chemical procedures and Mg isotope analysis by SN-MC-ICP-MS

Aliquots of 4 olivine RMs (SC-Ol, HN-Ol, IG-Ol, and OR-Ol) and all pyroxene RMs, weighing between 4 mg and 19 mg, were used for SN-MC-ICP-MS analysis.

All sample processing was performed under clean laboratory conditions in the Isotope Cosmochemistry and Geochronology Laboratory (ICGL) at Arizona State University (ASU). Each aliquot was cleaned by ultrasonication in Milli-Q® H_2O and then crushed using an agate mortar and pestle. These aliquots were dissolved using in-house distilled, high-purity acids. All olivine fractions were treated with 6 N HCl on a hotplate at 120 °C for 48 h followed by evaporation to dryness and further treated with a 3:1 mixture of HNO_3:HF at 120 °C for 24 h. After evaporating to dryness, a final treatment in 12 N HCl was used to ensure complete dissolution was achieved. The pyroxene fractions were digested in a 3:1 mixture of HNO_3:HF on a hotplate at 120 °C for 48 h followed by evaporation to dryness; this process was repeated until the sample was fully converted to fluorides. The fluorides were subsequently dissolved using 6 N HCl on the hotplate at 120 °C for 48 h. Following complete dissolution, a 1% fraction was taken from each aliquot for bulk chemical analysis on the iCAP-Q quadrupole ICP-MS at ASU.

A ~10 μg Mg equivalent fraction of each of the dissolved RM aliquots was loaded onto a quartz column packed with AG® 50W-X8 200–400 mesh cation resin. The Mg was purified using procedures similar to those described previously in Spivak-Birndorf et al. (2009). Following this chemical separation procedure, the Mg yields were verified using the iCAP-Q ICP-MS and were consistently >99%. The purified Mg cuts were dried and then brought into 250 ppb Mg solutions in 3% HNO_3 for analysis of Mg isotopes via SN-MC-ICP-MS.

Magnesium isotope analyses were performed on the ThermoFinnigan Neptune MC-ICP-MS in medium-resolution mode following procedures described in Spivak-Birndorf et al. (2009) and Bouvier et al. (2011). Instrumental mass fractionation was corrected by sample-standard bracketing using the DSM-3 Mg standard (Galy et al., 2003), and the mass-dependent Mg isotope composition of each RM is reported as $\delta^{25,26}$Mg values relative to this standard. To verify the accuracy and precision of our measured Mg isotope compositions, the USGS basaltic rock standard BCR-2 was processed through the entire chemical procedure alongside the olivine and pyroxene RMs and analyzed using the same SN-MC-ICP-MS protocols as these RMs during two analytical session. The reproducibility of our Mg isotope measurements was evaluated using repeat analyses of the DSM-3 Mg standard and the BCR-2 rock standard over the course of these two analytical sessions and was ±0.06‰ (2SD) and ±0.11‰ (2SD) for δ^{25}Mg and δ^{26}Mg, respectively.

Table 2
Summary of operating conditions of LA-MC-ICP-MS measurements.

Laser ablation system	
Laser type	Analyte-fs Ti:sapphire laser (Teledyne-Photon Machines)
Wavelength	266 nm
Pulse-width	~150 fs
Beam profile	Gaussian
Ablation cell	Two-volume HelEX (CETAC)
He gas flow	~0.55 L min^{-1} [a]
Ar make-up gas flow	~0.8 L min^{-1} [b]
Pulse energy at sample	15 μJ
Repetition rate	9–19 Hz
Ablation mode	Raster
Raster scan speed	2–10 μm/ s (typically 2 μm)
Raster iteration	1 pass
H_2O addition rate	12 or 40 μL/ min
MC-ICP-MS: Nu plasma II	
Mass resolution	Low mass resolution
Data collection mode	Time-resolved analysis (TRA) 0.2 s integrations
RF power	1300 W
Coolant Ar gas flow	13.2 L min^{-1}
Auxiliary Ar gas flow	0.8 L min^{-1}
^{24}Mg ion intensity	~3–5 V
On-peak gas blank	~60 s
Data acquisition time	~60 s

[a] Total He gas flow. Sub-equal amounts were delivered to the arm and the chamber.
[b] Total Ar flow. Sub-equal amounts were delivered from the nebulizer used for water addition and Ar delivered directly to the aerosol stream.

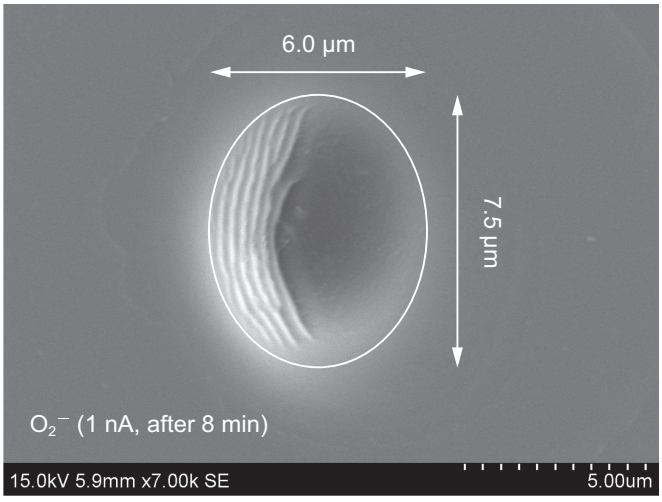

Fig. 1. A secondary electron image of an example of SIMS pit. This image was taken after Mg isotope analyses by using O_2^- primary ion beam (1 nA, session FI3). One analysis takes 8 min.

3.3. Mg isotope analysis by LA-MC-ICP-MS

Magnesium three-isotope analyses of 14 olivine RMs were made using a Nu plasma II MC-ICP-MS with a Nd:YLF-pumped Ti:sapphire femtosecond laser ablation (fs-LA) system at the University of Wisconsin-Madison. Typical operating conditions of fs-LA and MC-ICP-MS are summarized in Table 2. The laser spot size at the sample surface was ~13 μm in diameter as determined by the measured width of a line scan conducted using the laser and raster conditions reported in Table 2 on a grain of SC-Ol. For this laser ablation system, the laser spot size is controlled by adjusting the distance between sample and laser objective lens and by an adjustable iris placed before the objective lens. For each analysis, a raster ablation was used that ranged in size from ~1200 to 6000 $μm^2$ with various scan speeds (~2–10 μm/s) and laser repetition rates such that the dosage of laser shots delivered to a spot was similar using different conditions. These changes in laser repetition rate and raster settings were done so that the ion intensity of the RM's matched the ion intensity of the SC-Ol used as a bracketing standard. The ICP-MS was operated in low-mass-resolution mode using a 0.3 mm defining slit. Magnesium isotope ratios were measured using a standard-sample-bracketing method; SC-Ol grains ($Fo_{88.8}$) were used as the bracketing standard. A 60-second on-peak gas blank (laser not firing) was analyzed before each analysis, and this gas blank was subtracted from the signal analyzed for 60 s for both unknown samples and the bracketing standard. In general, fs-LA-MC-ICP-MS analysis have been adopted to overcome matrix effects compared with nanosecond laser ablation MC-ICP-MS analysis (e.g., Horn and von Blanckenburg, 2007; Steinhoefel et al., 2009; Oeser et al., 2014; Zheng et al., 2018). In this study, to further minimize possible matrix effects on fs-LA-MC-ICP-MS, Mg isotope analyses were performed under wet plasma conditions by co-aspirating ultra-pure water along with the ablated material into the plasma (Oeser et al., 2014). Two analysis sessions were conducted. During one session, ultra-pure water was introduced at a rate of 12 μL/min to a Peltier cooled (7 °C) cyclonic spray chamber (condition LA1) and in the second, water was aspirated at a rate of 40 μL/min (condition LA2). Typical $^{24}Mg^+$ intensities of SC-Ol under the condition LA1 and LA2 were 4.8 V and 2.9 V, respectively. The differences in ion intensities reflects the fact that instrument sensitivity is reduced as more water is added to the system (Zheng et al., 2018). The $\delta^{25}Mg$ external reproducibilities of the bracketing standard (SC-Ol) were ±0.08‰ (2SD) and ±0.17‰ (2SD) over the course of 12 h for condition LA1 and LA2, respectively. Mg isotope ratios of each RM were determined as $\delta^{25,26}Mg$ values relative to the SC-Ol bracket standard and these $\delta^{25,26}Mg$ values were normalized to DSM-3 scale by using $\delta^{25,26}Mg_{DSM\text{-}3}$ values of SC-Ol, as determined using SN-MC-ICP-MS analysis at IGCL, ASU.

3.4. Mg isotope analysis by MC-SIMS

Magnesium three-isotope analyses of olivine and pyroxene were performed in 4 sessions utilizing the WiscSIMS Cameca IMS 1280 at the University of Wisconsin-Madison equipped with a radio-frequency (RF) plasma ion source. We used two primary ion species (O^- and O_2^-), which were accelerated by 23 kV (−13 kV at the ion source and +10 kV at the sample surface) and were focused to ~9 or ~7.5 μm in diameter at 2.6 nA or 1 nA, respectively. Beam sizes were determined by SEM observations after SIMS analyses (Fig. 1). Secondary ion optics were adjusted to 200× magnification from the sample surface to the field aperture (4000 μm square) with a 50 eV energy window. Secondary Mg ions ($^{24}Mg^+$, $^{25}Mg^+$, $^{26}Mg^+$) were detected on multi-collector Faraday Cups (FCs) using one 10^{10} Ω and two 10^{11} Ω resistors for $^{24}Mg^+$, and $^{25,26}Mg^+$, respectively. The mass resolving power at 10% peak height was set to ~2500 (entrance slit; 90 μm and exit slit 500 μm) and contributions of $^{48}Ca^{2+}$ and $^{24}Mg^1H^+$ to ^{24}Mg and $^{25}Mg^+$ peaks were negligibly small. A typical mass spectrum is provided in Appendix EA2. The secondary ion optics are similar to that described in Kita et al. (2012) and Ushikubo et al. (2013). SC-Ol ($Fo_{88.8}$) grains were used as a bracketing standard for both olivine and pyroxene measurements. Typical $^{24}Mg^+$ count rates of SC-Ol by using O^- and O_2^- primary beams were ~2.4 × 10^8 and ~2.3 × 10^8 cps, respectively. Note that secondary ionization efficiency of Mg with O_2^- primary beam is higher than that with O^- primary beam (Kita et al., 2000). A single analysis takes 8 min, including 100 s of presputtering, ~80 s for automated centering of secondary beam (DTFA-X, DTFA-Y), and 300 s of integration (10 s × 30 cycle) of the secondary ion signals. The baseline of the FC detectors was monitored during each presputtering and averaged over eight analyses. External reproducibilities (2SD) of $\delta^{25}Mg_m$ and $\delta^{26}Mg_m$ were 0.10‰ and 0.17‰ for O^- analysis and 0.09‰ and

Table 3
Measured parameters used in this study.

Parameter	Method	Definition
Fo[a]	EPMA	Fo = Mg/[Mg + Fe] molar %
En[a]	EPMA	En = Mg/[Mg + Fe + Ca] molar %
Wo[a]	EPMA	Wo = Ca/[Mg + Fe + Ca] molar %
$\delta^{X}Mg_{DSM\text{-}3}$[b]	ICP-MS	$\delta^{X}Mg_{DSM\text{-}3} = [(^{X}Mg/^{24}Mg)_{RM}/(^{X}Mg/^{24}Mg)_{DSM\text{-}3} - 1] \times 1000$ (‰)
$\delta^{25}Mg_m$[c]	SIMS	$\delta^{25}Mg_m = [(^{25}Mg/^{24}Mg)_{RM}/0.12663 - 1] \times 1000$ (‰)
$f^*_{25\ (RM)}$	SIMS	$f^*_{25\ (RM)} = [(1 + \delta^{25}Mg_m/1000)/(1 + \delta^{25}Mg_{DSM\text{-}3}/1000) - 1] \times 1000$ (‰)
$bias^*_{25\ (RM\text{-}SCOl)}$	SIMS	$bias^*_{25\ (RM\text{-}SCOl)} = [(1 + f^*_{25\ (RM)}/1000)/(1 + f^*_{25\ (SCOl)}/1000) - 1] \times 1000$ (‰)
Mg/Si RSF[d]	SIMS	Mg/Si RSF = $(^{24}Mg^+/^{28}Si^+)$/(Mg cpfu/Si cpfu)

[a] Fo, En and Wo contents are calculated by considering total iron as ferrous iron.
[b] X = 25 or 26.
[c] Absolute $^{25}Mg/^{24}Mg$ ratio (=0.12663) is from Catanzaro et al. (1966).
[d] cpfu = cations per formula unit.

Table 4
Major and minor element compositions (wt%) of 17 olivine and 5 pyroxene RMs obtained by EPMA.

Sample name	EPMA session	Fo or En content	Na_2O	MgO	Al_2O_3	SiO_2	CaO	TiO_2	Cr_2O_3	FeO	NiO	MnO	Total
Olivine													
OR-Ol	2018 Aug & 2019 Jan.[a]	59.3	–	28.42	–	35.72	0.02	–	b.d.	34.81	b.d.	0.67	99.64
FJ-Ol	2018 Aug & 2019 Jan.[a]	73.4	–	37.24	–	37.63	0.06	–	b.d.	24.11	0.14	0.42	99.60
KN-Ol	2018 Aug & 2019 Jan.[a]	78.0	–	39.42	–	38.58	0.38	–	0.80	19.85	b.d.	0.42	99.45
CL09-19-Ol	2019 Jan.	79.4	–	41.41	–	38.26	0.08	–	b.d.	18.98	0.18	0.22	99.13
CL09-08-Ol	2019 Jan.	80.5	–	42.08	–	38.54	0.05	–	b.d.	18.13	0.29	0.24	99.33
SW-Ol	2018 Aug & 2019 Jan.[a]	81.8	–	42.87	–	38.91	b.d.	–	b.d.	16.99	b.d.	0.31	99.08
A77257-Ol	2019 Jan.	85.7	–	44.95	–	39.07	0.32	–	0.80	13.37	b.d.	0.46	98.97
CL09-33-Ol	2019 Jan.	86.6	–	46.19	–	39.17	0.06	–	b.d.	12.70	0.40	0.17	98.69
SC-Ol	2019 Jan.	88.8	–	48.22	–	40.01	0.07	–	b.d.	10.82	0.42	0.16	99.69
UWOL-1	2018 Aug & 2019 Jan.[a]	89.2	–	47.77	–	39.85	0.06	–	b.d.	10.27	0.41	0.14	98.50
IG-Ol	2019 Jan.	89.6	–	48.63	–	40.12	0.05	–	b.d.	10.09	0.42	0.16	99.48
HaK-Ol	2018 Aug & 2019 Jan.[a]	91.9	–	50.07	–	40.74	0.02	–	b.d.	7.92	0.51	0.10	99.36
WK-Ol	2018 Aug & 2019 Jan.[a]	94.3	–	51.44	–	41.17	0.12	–	0.23	5.54	0.47	0.09	99.05
WN-Ol	2018 Aug & 2019 Jan.[a]	95.5	–	53.63	–	41.80	b.d.	–	b.d.	4.49	b.d.	0.33	100.26
N7325-Ol	2019 Jan.	97.4	–	54.69	–	41.61	0.32	–	0.45	2.58	b.d.	0.12	99.77
SK-Ol	2019 Jan.	99.8	–	56.73	–	41.48	0.04	–	b.d.	0.19	b.d.	0.08	98.52
HN-Ol	2019 Jan.	100.0	–	57.31	–	42.04	b.d.	–	b.d.	b.d.	b.d.	b.d.	99.35
Pyroxene													
95AK-6 Di	2019 Sep.	48.6	0.10	17.92	0.92	54.91	25.41	b.d.	b.d.	1.26	–	0.07	100.59
IG-Cpx	2019 Sep.	48.6	0.50	16.70	4.52	51.70	22.51	0.45	0.91	2.65	–	0.09	100.05
JE En	2019 Sep.	85.5	b.d.	33.16	0.11	56.21	0.22	b.d.	b.d.	9.72	–	0.07	99.49
IG-Opx	2019 Sep.	88.9	b.d.	33.38	3.56	54.38	0.57	0.13	0.44	6.70	–	0.16	99.31
Sp79-11 En	2019 Sep.	96.3	b.d.	37.89	1.42	57.20	0.44	0.09	b.d.	2.03	–	0.41	99.49

b.d. (below detection limit).
– (not measured).
[a] Combined data obtained by two different sessions are summarized in this table. Fo content, MgO, SiO_2, CaO, FeO, and MnO are from session_2018Aug (Table EA3-1). Cr_2O_3 and NiO are from session_2019Jan. (Table EA3-2).

0.16‰ for O_2^- analysis, respectively.

We follow a data reduction scheme described in Ushikubo et al. (2017). Mass-dependent instrumental bias (f^*_{25} in the unit of ‰) of a RM is expressed as:

$$f^*_{25\,(RM)} = [(1 + \delta^{25}Mg_m/1000)/(1 + \delta^{25}Mg_{DSM-3}/1000)-1] \times 1000 \quad (1)$$

$\delta^{25}Mg_m$ represents a raw-measured, background-corrected $\delta^{25}Mg$ value of a RM measured by SIMS, which is expressed in δ-notation by normalizing to the absolute Mg isotope ratio ($^{25}Mg/^{24}Mg$ = 0.12663, Catanzaro et al., 1966). $\delta^{25}Mg_{DSM\text{-}3}$ represents a $\delta^{25}Mg$ value relative to DSM-3 that is determined by SN- or fs-LA-ICP-MS analyses. In order to correct instrumental drift during a SIMS session, the instrumental bias (f^*_{25}) of each RM was normalized to the bias of the running standard (SC-Ol). The relative bias* for a RM is defined as:

$$bias^*_{25\,(RM-SCOl)} = [(1 + f^*_{25\,(RM)}/1000)/(1 + f^*_{25\,(SCOl)}/1000)-1] \times 1000 \quad (2)$$

The $f^*_{25\ (SCOl)}$ represents an average f^*_{25} value that is calculated from eight bracket analyses of the running standard (SC-Ol) for each bracket. In general, instrumental mass bias is better-evaluated using $\delta^{26}Mg$ values because the mass difference between ^{24}Mg and ^{26}Mg isotopes is larger as compared to the difference between ^{24}Mg and ^{25}Mg isotopes. However, the fs-LA-MC-ICP-MS analyses were done at a mass resolving power of 400, which is insufficient to resolve $^{26}Mg^+$ from possible $^{12}C^{14}N^+$ and $^{52}Cr^{2+}$ isobars, making it challenging to assess the accuracy of $\delta^{26}Mg_{DSM\text{-}3}$ values determined by fs-LA. Thus we prefer to use $\delta^{25}Mg$ values to evaluate instrumental mass bias. Moreover, meteoritic olivine RMs may have excess radiogenic ^{26}Mg, making $\delta^{25}Mg$ values the best choice for evaluating IMF.

In addition to the above analysis conditions, a limited numbers of olivine RMs were analyzed for 300 cycles for each spot (~50 min) in order to examine the drift of f^*_{25} with the depth of the analysis. To obtain complete depth profile from the surface, only a short pre-sputtering time (10s) was applied and no secondary deflector adjustments (DTFA-X, DTFA-Y) were performed for these analyses. Secondary deflector adjustments for these analyses were performed on a spot adjacent to and just prior to the depth profile analysis.

Table 5
Mg isotope data of 17 olivine and 5 pyroxene RMs obtained by SN- and/or LA-MC-ICP-MS.

Sample name	Fo or En content[a]	SN-MC-ICP-MS								fs-LA-MC-ICP-MS			
		$\delta^{25}Mg_{DSM-3}$	2SD	2SE	$\delta^{26}Mg_{DSM-3}$	2SD	2SE	N[b]	Ref.	$\delta^{25}Mg_{DSM-3}$	2σ[c]	$\delta^{26}Mg_{DSM-3}$	2σ[c]
Standards													
DSM-3 250 ppb		0.00	0.06		0.00	0.11		147	This study				
Spex Mg		−1.08	0.04		−2.09	0.07		8	This study				
BCR-2		−0.05	0.08		−0.08	0.13		10	This study				
Olivine													
OR-Ol	59.3	−0.01	0.06		−0.02	0.13		27	This study	0.02	0.09	−0.05	0.24
FJ-Ol	73.4									−0.07	0.20	−0.10	0.30
KN-Ol	78.0									0.04	0.18	−0.01	0.30
SW-Ol	81.8									−0.02	0.14	−0.03	0.16
A77257-Ol	85.7									−0.07	0.14	−0.29	0.13
SC-Ol	88.8	−0.07	0.09		−0.15	0.16		10	This study				
UWOL-1	89.2									−0.14	0.10	−0.24	0.20
IG-Ol	89.6	−0.03	0.09		−0.05	0.15		10	This study	−0.08	0.18	−0.19	0.20
HaK-Ol	91.9									−0.06	0.13	−0.16	0.19
WK-Ol	94.3									−0.09	0.13	−0.17	0.20
WN-Ol	95.5									−0.04	0.09	−0.14	0.16
N7325-Ol	97.4									−0.07	0.14	−0.06	0.10
SK-Ol	99.8									−0.89	0.20	−1.72	0.54
HN-Ol	100.0	−0.37	0.09		−0.70	0.14		10	This study	−0.49	0.14	−0.95	0.17
Pyroxene													
95AK-6 Di	48.6	−0.74	0.05		−1.43	0.11		8	This study				
IG-Cpx	48.6	−0.14	0.10		−0.28	0.19		8	This study				
JE En	85.5	−0.26	0.06		−0.50	0.11		8	This study				
IG-Opx	88.9	−0.04	0.08		−0.07	0.13		8	This study				
Sp79-11 En	96.3	−0.06	0.05		−0.11	0.11		18	This study				
Olivine (literature data)													
CL09-19-Ol	79.4	−0.21	0.06		−0.37	0.06		2	[1]				
CL09-08-Ol	80.5	−0.21	0.05		−0.41	0.07		4	[1]				
CL09-33-Ol	86.6	−0.25	0.05		−0.47	0.06		2	[1]				
Springwater olivine		−0.11		0.03	−0.22		0.04	7	[2]				
NWA 7325 olivine		−0.16		0.02	−0.23		0.04	6	[3]				

References; [1] Xiao et al. (2013); [2] Handler et al. (2009); [3] Koefoed et al. (2016).
[a] Molar % of forsterite or enstatite end-members based on EPMA analyses performed in this study
[b] Number of analyses
[c] 2σ errors (‰) are propagated both 2SD of fs-LA-MC-ICP-MS analyses and 2SE of $\delta^{25}Mg_{DSM-3}$ (SC-Ol) obtained by SN-MC-ICP-MS analyses.

3.5. Major and minor element analyses by SIMS

Major and minor element analyses (Na, Mg, Al, Si, Ca, Cr, Mn, Fe, and Ni) of 17 olivine RMs were performed with the WiscSIMS Cameca IMS 1280. As with the case for Mg isotope analysis, two different primary ion species (O^- and O_2^-) were used, which were focused to ~2 or ~1.5 μm diameter at 16 pA or 6 pA, respectively. Secondary ion optics was operated under the same conditions for Mg isotope analysis described in Section 3.4, except for the mass resolving power that was set to ~3000. A secondary $^{24}Mg^+$ ion was detected by an axial FC (FC2) with a 10^{11} Ω resistor and the other secondary ions ($^{23}Na^+$, $^{27}Al^+$, $^{28}Si^+$, $^{40}Ca^+$, $^{52}Cr^+$, $^{55}Mn^+$, $^{56}Fe^+$, and $^{60}Ni^+$) and the mass 22.7 for stabilizing magnetic field for $^{23}Na^+$ were detected by an axial electron multiplier (EM) with magnetic peak jumping mode. SC-Ol grains were used as a running standard. Typical $^{24}Mg^+$ count rates of SC-Ol for O^- and O_2^- analyses were ~8.5×10^5 and ~8.6×10^5 cps, respectively. Per cycle, the count duration for $^{24}Mg^+$, $^{28}Si^+$, and $^{56}Fe^+$ ions were 2 s, and for the mass 22.7 and $^{23}Na^+$, $^{27}Al^+$, $^{40}Ca^+$, $^{52}Cr^+$, $^{55}Mn^+$, and $^{60}Ni^+$ ions were 1 s. The waiting duration for $^{23}Na^+$, $^{27}Al^+$, $^{28}Si^+$, $^{55}Mn^+$, $^{56}Fe^+$, and $^{60}Ni^+$ ions were 1.6 s, for $^{24}Mg^+$ and $^{52}Cr^+$ ions were 2.4 s, for the $^{40}Ca^+$ ion was 3.0 s, and for the mass 22.7 was 2.0 s. A single analysis takes 6 min, including 100 s of presputtering, ~80 s for automated centering of secondary beam (DTFA-X, DTFA-Y), and 160 s of integration (32 s × 5 cycle) of the secondary ion signals.

For SIMS analyses, an ion yield of Mg (or Si) is defined as count rate (per second) of Mg (or Si) divided by primary ion beam intensity (nA). A relative sensitivity factor (RSF) of the $^{24}Mg^+/^{28}Si^+$ ratio (hereafter referred as Mg/Si RSF) is expressed as

$$\text{Mg/Si RSF} = (^{24}Mg^+/^{28}Si^+)/(\text{Mg cpfu/Si cpfu}) \quad (3)$$

where ($^{24}Mg^+/^{28}Si^+$) is a ratio of count rates of secondary ions $^{24}Mg^+$ and $^{28}Si^+$, and Mg (or Si) cpfu represents a number of cations of Mg (or Si) per oxygen in the oxide formula, which is determined by EPMA analyses.

4. Results

Definitions of measured parameters used in the following are summarized in Table 3.

4.1. EPMA analyses

Representative chemical compositions of olivine and pyroxene RMs are summarized in Table 4. Complete electron microprobe data of olivine and pyroxene RMs are given in Appendix EA3. Electron microprobe data were collected during three analytical sessions. The first session (August 2018) was carried out to evaluate the Fo homogeneity of 8 olivine RMs (Table EA3-1). The second session (January 2019) was carried out to evaluate Fo homogeneity of additional 9 olivine RMs (Table EA3-1) and to determine minor element abundances including Cr and Ni in all of olivine RMs (Table EA3-2). The third session (September 2019) was carried out to determine the major and minor element compositions and homogeneity of all pyroxene RMs (Table EA3-1). Homogeneities of Fo and En contents are summarized in Appendix

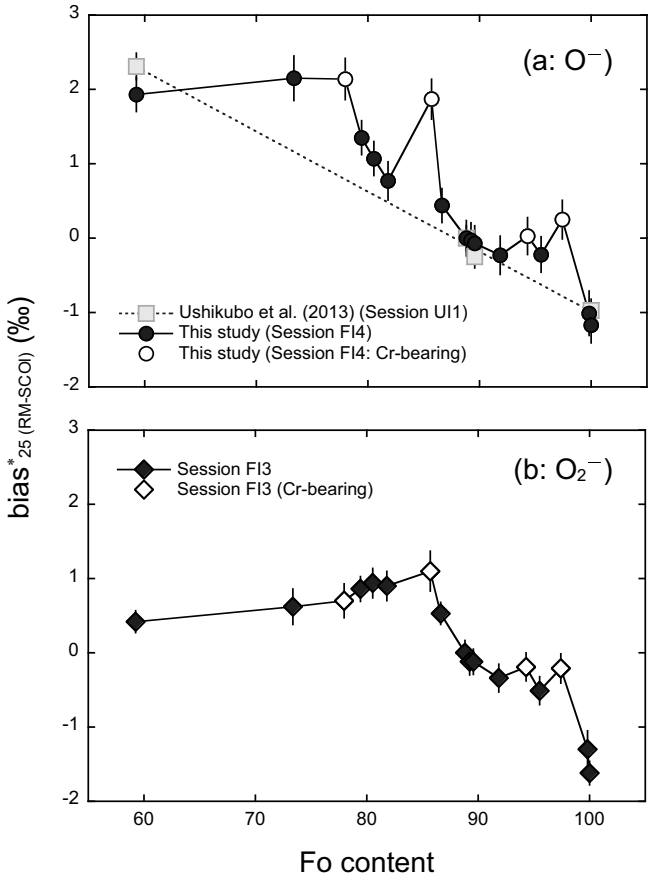

Fig. 2. The bias*$_{25\ (RM\text{-}SCOl)}$ values of 17 olivine RMs obtained by (a) O^- and (b) O_2^- analyses as a function of Fo content. The dashed line in Fig. 2a represents the best-fit line for data obtained by using the Duoplasmatron source reported in Ushikubo et al. (2013). Cr-bearing (~0.8 wt% in Cr_2O_3) RMs tend to show higher bias*$_{25\ (RM\text{-}SCOl)}$ values relative to those of RMs with similar Fo contents, except for KN-Ol ($Fo_{78.0}$). Errors are 2σ.

EA4. The Fo contents of 17 olivine RMs and the En contents of 5 pyroxene RMs range from 59.3 to 100 and 48.6 to 96.3, respectively. Variations in Fo or En contents for each olivine or pyroxene RM are within ±0.7 unit (1SD) and most of them are within ±0.3 unit (1SD).

4.2. SN- and LA-MC-ICP-MS analyses

The Mg isotope ratios of the USGS basaltic rock standard (BCR-2), 4 olivine (HN-Ol, IG-Ol, SC-Ol, and OR-Ol), and 5 pyroxene (Sp79-11, IG-Opx, IG-Cpx, JE En, and 95AK-6) RMs analyzed by SN-MC-ICP-MS are reported as $\delta^{25,26}Mg_{DSM\text{-}3}$ values (Table 5). The $\delta^{25,26}Mg_{DSM\text{-}3}$ values of 3 olivine RMs (CL09-08-Ol, CL09-19-Ol, and CL09-33-Ol) which have been determined by Xiao et al. (2013) are also shown in Table 5. The BCR-2 standard resulted in $\delta^{25}Mg_{DSM\text{-}3} = -0.05 \pm 0.08$‰ (2SD), which is in agreement with the recommended value ($\delta^{25}Mg_{DSM\text{-}3} = -0.12 \pm 0.02$‰, 2SD; Teng, 2017) within uncertainties. Four olivine and 5 pyroxene RMs have $\delta^{25}Mg_{DSM\text{-}3}$ values ranging from -0.37 ± 0.09‰ to -0.01 ± 0.06‰ and -0.74 ± 0.05‰ to -0.04 ± 0.08‰ (2SD), respectively. The $\delta^{25}Mg_{DSM\text{-}3}$ value of the SC-Ol is determined to be -0.07 ± 0.09‰ (2SD), which is also in agreement with the average value of San Carlos olivine ($\delta^{25}Mg_{DSM\text{-}3} = -0.13 \pm 0.03$‰, 2SD) reported in Hu et al. (2016b).

We analyzed 14 olivine RMs by fs-LA-MC-ICP-MS under the two different analytical conditions (LA1 and LA2, see the Section 3.3). Under the condition LA1, $\delta^{25}Mg_{DSM\text{-}3}$ values of OR-Ol ($Fo_{59.3}$) and IG-Ol ($Fo_{89.6}$) are determined to be -0.06 ± 0.08‰ (2SD) and -0.04 ± 0.05‰ (2SD), respectively, which are consistent with those obtained by SN-MC-ICP-MS (-0.01 ± 0.06‰ (2SD) and -0.03 ± 0.09‰ (2SD), respectively). $\delta^{25}Mg_{DSM\text{-}3}$ values of SW-Ol ($Fo_{81.8}$) from the Springwater meteorite and N7325-Ol ($Fo_{97.4}$) from the NWA 7325 meteorite are determined to be -0.09 ± 0.06‰ and -0.32 ± 0.07‰ (2SD), respectively. The $\delta^{25}Mg_{DSM\text{-}3}$ value of SW-Ol is also agreement with a literature value (-0.11 ± 0.03‰, 2SE; Handler et al., 2009). However, the $\delta^{25}Mg_{DSM\text{-}3}$ value of N7325-Ol with high $Fo_{97.4}$ is ~0.16‰ lower than a literature value (-0.16 ± 0.02‰, 2SE; Koefoed et al., 2016). Interestingly, the $\delta^{25}Mg_{DSM\text{-}3}$ value of WN-Ol with high $Fo_{95.5}$ from the Winona meteorite, is -0.29 ± 0.07‰ (2SD), which is also ~0.14‰ lower than that of a bulk Winona meteorite (-0.15 ± 0.04‰, 2SD; Sedaghatpour and Teng, 2016). Although it is possible that Mg isotope ratios of WN-Ol and the bulk Winona meteorite are different, the low $\delta^{25}Mg_{DSM\text{-}3}$ values observed in high Fo samples relative to the literature values suggest that small extent of matrix effects (~0.16‰/amu) exist on fs-LA-MC-ICP-MS analyses of olivine with high Mg contents under the condition LA1.

In order to overcome the problem, we introduced more water to the ICP (40 μL/min, condition LA2) compare to the condition LA1 (12 μL/min). The Mg isotope ratios of 13 olivine RMs analyzed under the condition LA2 are reported as $\delta^{25,26}Mg_{DSM\text{-}3}$ values in Table 5. Thirteen olivine RMs have $\delta^{25}Mg_{DSM\text{-}3}$ values ranging from -0.89 ± 0.20‰ to 0.04 ± 0.17‰ (2SD). For comparison, $\delta^{25,26}Mg_{DSM\text{-}3}$ values of olivine grains from the Springwater and NWA 7325 meteorites, which have been determined by Handler et al. (2009) and Koefoed et al. (2016), respectively, are also shown in Table 5. Under the condition LA2, high Fo content samples (WN-Ol and N7325-Ol) have greater $\delta^{25}Mg_{DSM\text{-}3}$ values (-0.04 ± 0.08‰ (2SD) and -0.07 ± 0.14‰ (2SD), respectively) relative to those obtained using LA1 conditions. The $\delta^{25}Mg_{DSM\text{-}3}$ values for these forsteritic olivines measured using LA2 conditions agree with the literature values of the bulk Winona meteorite (Sedaghatpour and Teng, 2016) and olivine from NWA 7325 meteorite (Koefoed et al., 2016), respectively. Likewise, $\delta^{25}Mg_{DSM\text{-}3}$ values determined using LA2 conditions for OR-Ol ($Fo_{59.3}$), IG-Ol ($Fo_{89.5}$), and HN-Ol (Fo_{100}) are consistent with those obtained by SN-MC-ICP-MS within 2SD uncertainties (see Table. 5). The lower precision obtained for LA2 is likely driven by the decrease in sensitivity associated with the large amount of water co-aspirated with the ablated material as compared to LA1 conditions. The consistency between fs-LA- and SN-MC-ICP-MS results verifies no significant matrix effects on fs-LA-MC-ICP-MS measurements within analytical uncertainties (≤0.20‰ in $\delta^{25}Mg$, 2SD) under LA2 conditions.

4.3. SIMS analyses

4.3.1. Instrumental bias of olivine RMs

Multiple sessions of SIMS Mg isotope analysis were conducted (Appendix EA5). Olivine RMs were evaluated for Mg isotope heterogeneities by conducting multiple grain analyses (Appendix EA4). The measured $\delta^{25}Mg_m$ values of each olivine RM had limited variability (≤0.23‰, 2SD). The f^*_{25} and bias*$_{25\ (RM\text{-}SCOl)}$ values of all RMs are shown in Table 6 and complete SIMS Mg isotope data for each session are provided in Appendix EA6.

Correction for IMF of isotope ratio analysis by SIMS is typically done by applying an empirical correction. This empirical correction is established by determining a calibration line or curve of IMF values for standards that have a range of major element compositions (e.g., Eiler et al., 1997; Valley and Kita, 2009; Kita et al., 2012; Śliwiński et al., 2016a, 2016b, 2018; Isa et al., 2017; Chaussidon et al., 2017; Scicchitano et al., 2018). The IMF for the 17 olivine RMs that range from Fo_{59} to Fo_{100} defined a ~3‰ range of f^*_{25} values. The f^*_{25} value for olivine analyses using a O^- primary beam ranged from −3.5 to −0.3‰, and from −3.5 to −0.7‰ using an O_2^- primary beam (Table 6). The bias*$_{25\ (RM\text{-}SCOl)}$ values of 17 olivine RMs defines a complex function versus Fo content. This function is slightly different if an O^- or O_2^- primary ion beam is used (Fig. 2a and b, respectively). In

Table 6
SIMS δ^{25}Mg instrumental biases of 17 olivine and 5 pyroxene RMs and ($^{24}Mg^+/^{28}Si^+$)/Fo values of 17 olivine RMs.

Sample name	Fo or En content	Session_UI1 and UI2 (Duo O^-)				Session_FI4 (RF O^-)			Session_FI3 (RF O_2^-)			Session_FE2 (RF O^-)		Session_FE1 (RF O_2^-)	
		$f^*_{25\ (RM)}$ (‰)	bias$^*_{25\ (RM\text{-}SCOl)}$ (‰)	2 σ[a]	Ref.	$f^*_{25\ (RM)}$ (‰)	bias$^*_{25\ (RM\text{-}SCOl)}$ (‰)	2 σ[a]	$f^*_{25\ (RM)}$ (‰)	bias$^*_{25\ (RM\text{-}SCOl)}$ (‰)	2 σ[a]	($^{24}Mg^+/^{28}Si^+$)/Fo (× 100)	2 σ[b]	($^{24}Mg^+/^{28}Si^+$)/Fo (× 100)	2 σ[b]
Olivine															
OR-Ol	59.3	−0.54	2.31	0.18	[1]	−0.49	1.93	0.23	−1.44	0.42	0.15	8.74	0.78	12.45	0.57
FJ-Ol	73.4					−0.27	2.15	0.30	−1.23	0.62	0.24	8.85	0.29	12.25	0.48
KN-Ol	78.0					−0.27	2.14	0.28	−1.18	0.70	0.23	8.86	0.39	11.92	0.51
CL09-19-Ol	79.4					−1.26	1.35	0.23	−0.94	0.86	0.17	7.59	0.36	11.67	0.46
CL09-08-Ol	80.5					−1.53	1.07	0.23	−0.86	0.94	0.20	7.10	0.35	11.73	0.48
SW-Ol	81.8					−1.60	0.77	0.26	−0.97	0.90	0.20	6.77	0.18	11.78	0.45
A77257-Ol	85.7					−0.63	1.87	0.27	−0.72	1.10	0.27	7.70	0.24	11.45	0.47
CL09-33-Ol	86.6					−2.16	0.44	0.23	−1.31	0.53	0.15	5.89	0.16	9.71	0.43
SC-Ol	88.8	−2.84	0.00	0.17	[1]	−2.41	0.00	0.24	−1.83	0.00	0.17	5.59	0.15	9.11	0.29
UWOL-1	89.2					−2.39	−0.03	0.24	−2.01	−0.12	0.18	5.55	0.28	9.04	0.29
IG-Ol	89.6	−3.09	−0.25	0.15	[1]	−2.67	−0.07	0.24	−1.96	−0.12	0.17	5.52	0.16	8.75	0.32
HaK-Ol	91.9					−2.61	−0.23	0.26	−2.22	−0.34	0.19	5.38	0.15	8.28	0.26
WK-Ol	94.3					−2.38	0.03	0.25	−2.00	−0.19	0.19	5.63	0.15	8.57	0.31
WN-Ol	95.5					−2.62	−0.22	0.24	−2.31	−0.51	0.19	5.55	0.19	8.04	0.26
N7325-Ol	97.4					−2.07	0.25	0.26	−1.98	−0.21	0.20	5.87	0.27	8.57	0.27
SK-Ol	99.8					−3.35	−1.01	0.30	−3.14	−1.30	0.25	5.46	0.24	7.75	0.25
HN-Ol	100.0	−3.80	−0.97	0.15	[1]	−3.54	−1.17	0.24	−3.49	−1.62	0.16	5.40	0.23	7.55	0.24
Pyroxene															
95AK-6 Di	48.6	0.83	3.72	0.18	[2]				0.00	1.81	0.18				
IG-Cpx	48.6	1.33	4.23	0.19	[2]				0.55	2.36	0.17				
JE En	85.5	0.43	3.42	0.15	[1]				1.28	3.09	0.15				
IG-Opx	88.9	0.39	3.38	0.24	[1]				1.41	3.22	0.24				
Sp79-11 En	96.3	−0.27	2.72	0.15	[1]				0.65	2.46	0.15				

References; [1] Ushikubo et al. (2013); [2] Ushikubo et al. (2017). All data from Ushikubo et al. (2013, 2017) were renormalized to DSM-3 scale using SN-MC-ICP-MS results.

[a] 2σ error (‰) = $\sqrt{(2SD_{SIMS})^2 + (2SD_{ICPMS})^2}$, where $2SD_{SIMS}$ represents either δ^{25}Mg homogeneity of each RM or long-term reproducibility of the running standard (SC-Ol), whichever is larger.

[b] 2σ error represents either 2 standard error (2SE) of each measurement or long-term reproducibility (2SD) of the running standard (SC-Ol), whichever is larger.

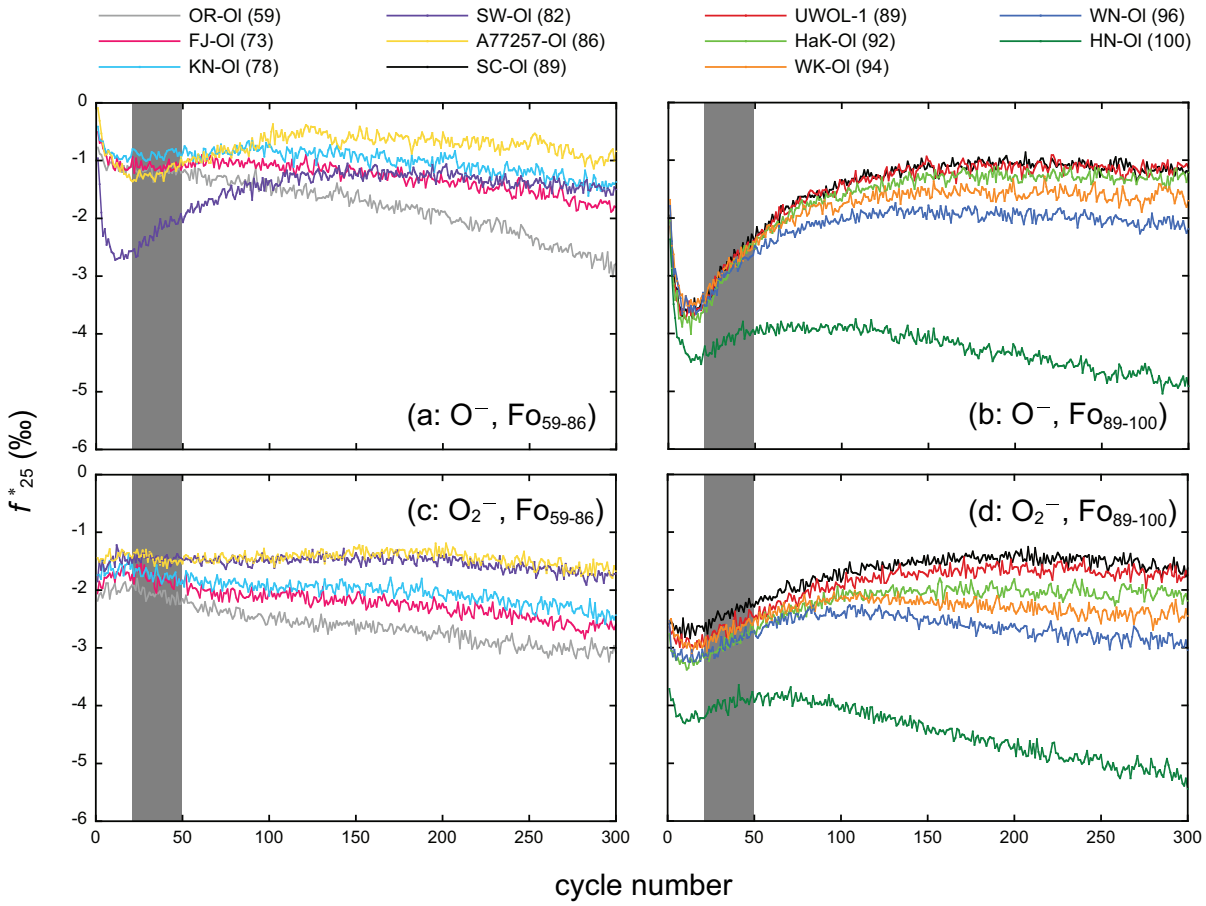

Fig. 3. The f^*_{25} values of 11 olivine RMs for (a and b) O^- and (c and d) O_2^- analyses against cycle number. One cycle takes 10 s so that one analysis (300 cycles) takes ~50 min. Gray bands represent cycle numbers correspond to depths that Mg isotope data (listed in Table 6) were obtained.

general, bias$^*_{25\ (RM\text{-}SCOl)}$ values are maximum at around Fo_{80} and are lowest for near-pure forsterite RMs (SK-Ol and HN-Ol). The change in IMF for olivine from Fo_{59} to Fo_{80} is approximately 1‰. There is a 3‰ change in IMF from Fo_{80} to Fo_{100}, but this change is not a smooth function of Fo content. In the case of O^- analysis, A77257-Ol ($Fo_{85.7}$) shows the bias$^*_{25\ (RM\text{-}SCOl)}$ value ~1.5‰ higher those of RMs with similar Fo contents (Fig. 2a). The same RM shows a slightly enhanced bias$^*_{25\ (RM\text{-}SCOl)}$ value if an O_2^- primary beam was used (Fig. 2b). In both primary beam conditions, the bias$^*_{25\ (RM\text{-}SCOl)}$ values zigzag between Fo_{89} and Fo_{97}, and decrease by ~1‰ at Fo_{100}. We conducted four sessions of SIMS Mg isotope analyses (FI1 and FI3 with O_2^- and FI2 and FI4 with O^-) and confirmed that the complex relationship between IMFs and Fo contents was reproduced. The comparisons of the relationships between IMF and Fo content obtained from each session are shown in Appendix EA6. Overall, the complex instrumental biases against Fo content observed in 17 olivine RMs suggest that the instrumental bias on olivine is not entirely controlled by Mg and Fe contents.

Eleven olivine RMs were analyzed for a longer analysis time (total 300 cycles, ~50 min) to determine the changes of IMF as a function of the depth of sputtering. The results are shown in Fig. 3a–d as f^*_{25} values versus analysis cycle numbers. During the first 100 cycles (1000 s) there are large changes in f^*_{25} values, especially for O^- analysis (Fig. 3a–b). For the rest of the cycles, f^*_{25} values is nearly constant or monotonically decreasing. Fig. 4a and b show the average bias$^*_{25\ (RM\text{-}SCOl)}$ values for each depth (per 50 cycles) as a function of Fo content. In both O^- and O_2^- analyses, the bias$^*_{25\ (RM\text{-}SCOl)}$ values for first ~100 cycles are not a smooth function of Fo content and those for after 100 cycles tend to be smoother than those for first ~100 cycles.

4.3.2. Ion yields of Mg and Si among olivine RMs

Results of SIMS major and minor element analyses of olivine RMs are listed in Appendix EA7. We examined the variations in ion yields of Mg and Si among 17 olivine RMs (Fig. 5a–d). Ion yields of Mg are not positively correlated with Fo content and show a complex behavior as a function of Fo content (Fig. 5a–b). Ion yields of Si vary by ~33% and ~26% for O^- and O_2^- analyses, respectively (Fig. 5c–d). In the case of O^- and O_2^- analysis, Si ion yield of olivine RMs with $Fo_{59.3}$ to $Fo_{78.0}$ decreases with Fo content, whereas Si ion yield increases in RMs from $Fo_{78.0}$ to $Fo_{91.9}$, except for A77257-Ol ($Fo_{85.7}$). The Si ion yield for RMs with Fo contents from $Fo_{91.9}$ to Fo_{100} defines a complex behavior. For analyses done using a O^- primary beam the Si ion yield largely decreases but for analysis done with a O_2^- primary beam the Si ion yield defines a "zig-zag" pattern showing an overall decrease in Si ion yield (Fig. 5c–d). We do not find a complex behavior for Fe^+ yields against Fo contents (see Appendix EA7).

The ion yields of Mg^+ and Si^+ may also change depending on the sputter-rate of each RM that would differ by Fo contents (e.g., Isa et al., 2017). Thus, we calculate RSFs of secondary ion yields $^{24}Mg^+/^{28}Si^+$ ratios in Fig. 5e–f. The Mg/Si RSF is a complex function of Fo content and it is very similar to the trend in bias$^*_{25\ (RM\text{-}SCOl)}$ as a function of Fo content (Fig. 2a–b). The Mg/Si RSFs are nearly constant for RMs with $Fo_{59.3}$ to $Fo_{78.0}$ or from $Fo_{59.3}$ to $Fo_{85.7}$ for O^- or O_2^- analyses, respectively. The Mg/Si RSFs are negatively correlated with olivine RMs of Fo $_{78.0}$ to $Fo_{91.9}$ (at the exception of A77257-Ol) or from $Fo_{85.7}$ to $Fo_{91.9}$ for O^- or O_2^- analyses, respectively. The exact same systematic is observed in bias$^*_{25\ (RM\text{-}SCOl)}$. Moreover, irregularity of Mg/Si RSFs against Fo content follows that of bias$^*_{25\ (RM\text{-}SCOl)}$, such as A77257-Ol ($Fo_{85.7}$), WK-Ol ($Fo_{94.3}$), WN-Ol ($Fo_{95.5}$), and N7325-Ol ($Fo_{97.4}$) for both O^- or O_2^- analyses.

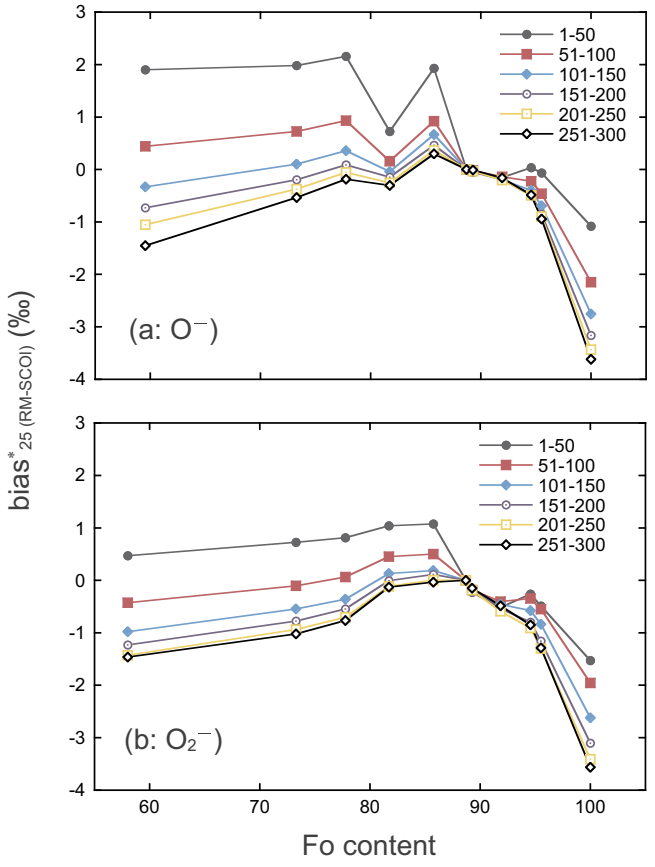

Fig. 4. The bias*$_{25\ (RM\text{-}SCOl)}$ values of 11 olivine RMs with different depths obtained by (a) O^- and (b) O_2^- analyses as a function of Fo content. The different symbols and lines represent the average of 50 cycles taken over the total 300 cycle analysis. Error bars are not shown for clarity, but would typically be ±0.5‰ (2SD), except for the first 100 cycles of O^- analysis that show large changes in f^*_{25} values (Fig. 3a–b) so that errors are larger (~1‰) than those for the rest of the cycles.

4.3.3. Instrumental bias of pyroxene RMs

Five pyroxene RMs that range from $En_{48.6}$ to $En_{96.3}$ were analyzed for their Mg isotope ratios using an O_2^- primary beam and the IMF, (f^*_{25}), ranged from 0 to 1.4‰ (Table 6). The range of the pyroxene IMF (1.4‰/amu for $En_{48.6}$ to $En_{96.3}$) is two times smaller than the IMF determined for the olivine RMs (3.3‰/amu for $Fo_{59.3}$ to Fo_{100}). However, the absolute magnitude of the IMF for the pyroxene RMs is more positive than the IMF for the olivine RMs (Table 6). The bias*$_{25\ (RM\text{-}SCOl)}$ values of three orthopyroxene RMs (JE En, IG-Opx, and Sp79-11 En) are not a smooth function of En content (Fig. 6). The two clinopyroxene RMs, IG-Cpx and 95AK-6 Di, have identical En content ($En_{48.6}$) but the bias*$_{25\ (RM\text{-}SCOl)}$ value of IG-Cpx is ~0.5‰ higher than that bias value of 95AK-6 Di.

5. Discussion

5.1. Matrix effects on SIMS Mg isotope analysis of olivine and pyroxene

5.1.1. Instrumental bias of olivine and calibration against Fo contents

Longer SIMS Mg isotope analyses (total 300 cycles, ~50 min) of 11 olivine RMs show significant IMF changes (f^*_{25}, up to ~2.9‰) as a function of sputtering depth (Fig. 3a–d). The present results suggest that instrumental biases with different depth should be characterized for depth profiling Mg isotope analysis of olivine even if samples have homogeneous chemical compositions. The depth-dependent IMF changes also indicate that the IMF behaves differently depending on different analytical conditions such as primary beam current, beam size, integration time, and cycle numbers.

For olivine RMs with $Fo_{59.3}$ to $Fo_{78.0}$, the instrumental biases on both O^- and O_2^- analyses varies by ≤0.3‰/amu. Thus, both accurate and precise Mg isotope analysis of olivine with low Fo can be performed. Moreover, Mg/Si RSFs of these low Fo content olivine RMs are near-constant (Fig. 5e–f), suggesting no irregular behavior of secondary ion generation of Mg and Si. For olivine with Fo > 78.0, instrumental biases range over ~3‰/amu and this variability is a complex function of the olivine Fo content. Fitting the variation of IMF as a function of Fo content would result in a poor fit to these data indicating that the IMF is not solely a function of Fo content.

As noted previously, the variation in Mg/Si RSFs as a function of Fo content and the variation in IMF as a function of Fo content are similar, and we consider this to imply that the variations in IMF are in part a result in changes in the ionization efficiency of Mg and Si. The complex relationship between Mg and Si ion yields and Mg and Si contents has been observed in other studies (Steele et al., 1981; Chaussidon et al., 2017; Villeneuve et al., 2019). For example, Villeneuve et al. (2019) found large matrix effects on Si ion yield and instrumental mass fractionation in SIMS Si isotope analysis of olivine and low-Ca pyroxene using two different primary ion species (Cs^+ and O^-). In both cases, relationships between Si ion yield of olivine as a function of Fo content changed at ~$Fo_{80,}$ although the trends for Cs^+ and O^- analyses were in opposite directions (see Fig. 2 in Villeneuve et al., 2019). The reasons for such complex instrumental bias and ionization efficiency are not well understood (Villeneuve et al., 2019). The observed relationships between ion yields of Mg^+ and Si^+ and Fo content in this study are broadly consistent with the results for O^- analyses by Chaussidon et al. (2017) and Villeneuve et al. (2019). However, previous studies did not include olivine RMs similar to A77257-Ol ($Fo_{85.7}$) and Mg-rich samples (Fo > 95) that resulted in a significant irregularities in bias*$_{25\ (RM\text{-}SCOl)}$ against Fo content as observed in this work.

5.1.2. Effect of minor element concentrations in olivine

Olivine RMs with higher Cr concentrations (Cr_2O_3 > 0.2 wt%) tend to have higher bias*$_{25\ (RM\text{-}SCOl)}$ values relative to those of olivine RMs without Cr (Fig. 2a–b). Many meteoritic olivine samples, in which Cr occurs as divalent cation (Cr^{2+}) under relatively reducing conditions, tend to have higher Cr contents as compared to terrestrial olivine samples. As shown in Fig. 2a–b, Cr-bearing olivine RMs (Cr_2O_3 > 0.2 wt%) tend to show larger bias*$_{25\ (RM\text{-}SCOl)}$ values relative to those of olivine RMs with similar Fo contents, although this is not the case for all of them. Fig. 7 shows the difference between bias*$_{25\ (RM\text{-}SCOl)}$ values of Cr-bearing olivine RMs compared to mean bias*$_{25\ (RM\text{-}SCOl)}$ values of other olivine RMs with similar Fo contents (hereafter referred as residual bias). The detail calculation of the residual biases are shown in Appendix EA8. In the case of O^- analysis, the residual biases of Cr-bearing olivine RMs with Fo contents ≥ 86 are positively correlated with Cr_2O_3 contents (Fig. 7), and those with Fo ≥ 94 for O_2^- analysis follow a similar correlation (Fig. 7). The other Cr-bearing olivine RMs with lower Fo contents (Fo_{78} for O^- and Fo_{86} and greater for O_2^-) do not follow these correlations. Note that both the IMF and Mg/Si RSFs as a function of Fo content (Fig. 5e–f) are nearly constant for olivine with a Fo content below Fo_{78} for O^- and Fo_{86} for O_2^-, suggesting that secondary ionization processes are not sensitive to sample matrix below these Fo contents. In contrast, small changes in Cr contents (<1 wt% as Cr_2O_3) in Mg-rich olivine (Fo > 78 for O^- and >86 for O_2^-) might drastically change the secondary ionization yields and bias*$_{25\ (RM\text{-}SCOl)}$ values. These observations suggest that the secondary ionization process is sensitive to sample matrix in Mg-rich olivine.

5.1.3. Alternative bias correction scheme for olivine

Here, we explore an alternate calibration scheme using the ion yield $^{24}Mg^+/^{28}Si^+$ ratios for the bias*$_{25\ (RM\text{-}SCOl)}$ values. Fig. 8a and b show the relationships between bias*$_{25\ (RM\text{-}SCOl)}$ and $^{24}Mg^+/^{28}Si^+$ ratio

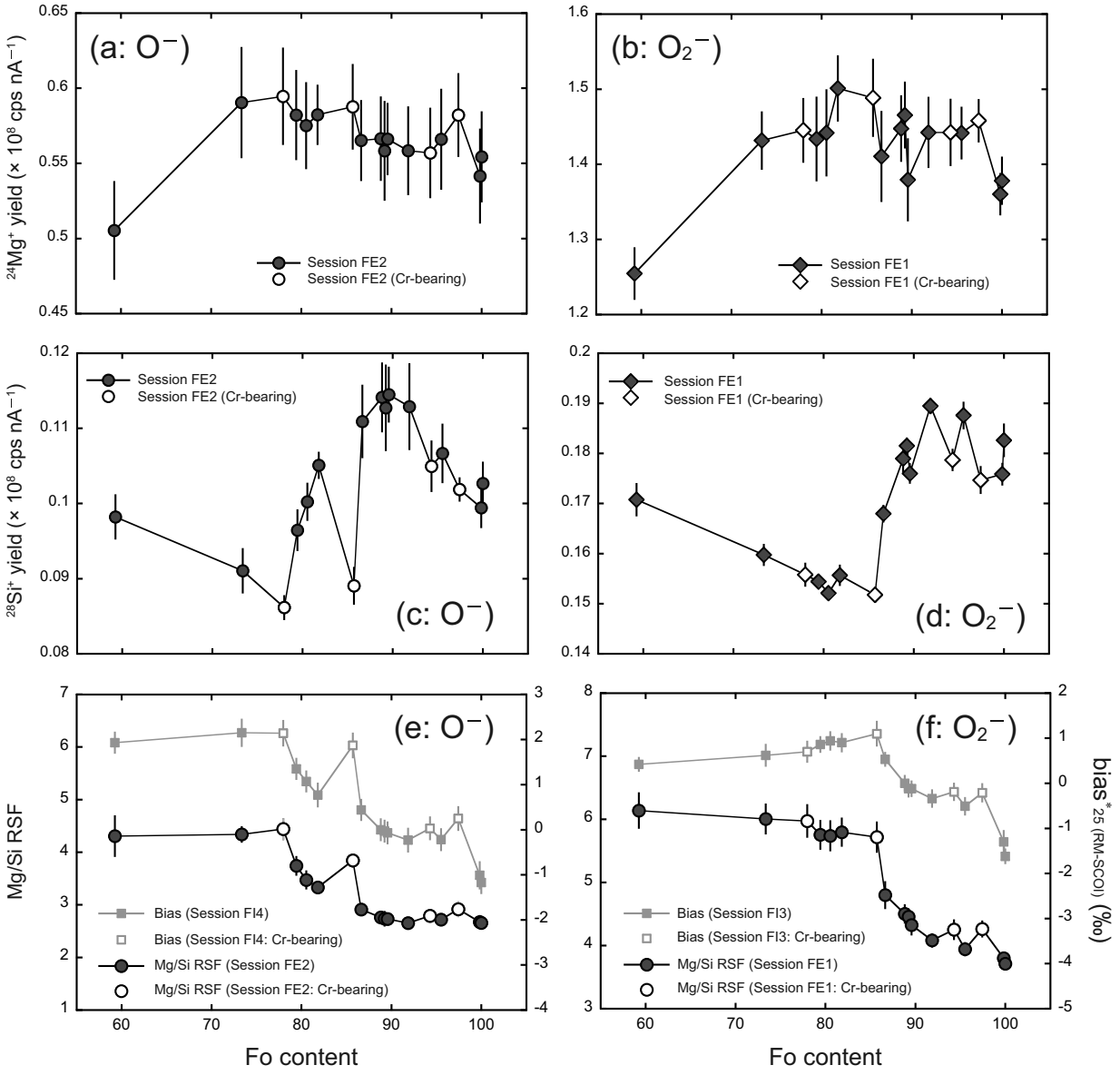

Fig. 5. Compositional dependences of secondary ion yields and relative sensitivities of Mg^+/Si^+ as a function of olivine Fo content. (a, b) Secondary $^{24}Mg^+$ ion yields vs. Fo contents for O^- and O_2^- analyses, respectively. (c, d) Secondary $^{28}Si^+$ ion yields vs. Fo contents for O^- and O_2^- analyses, respectively. (e, f) Relative sensitivity factors of Mg^+/Si^+ (Mg/Si RSFs) vs. Fo contents for O^- and O_2^- analyses, respectively. Errors of ion yields and Mg/Si RSFs are 2SE. For comparison, the bias*$_{25\ (RM\text{-}SCOl)}$ values of 17 olivine RMs as shown in Fig. 2a and b are also plotted as gray square symbols. Errors of the bias*$_{25\ (RM\text{-}SCOl)}$ values are 2σ. Yield = count rate (per second)/primary ion beam intensity (nA). Mg/Si RSF = ($^{24}Mg^+/^{28}Si^+$)/(Mg cpfu/Si cpfu).

divided by Fo content. Since olivine should have near-constant Si atomic abundances, differences in the $^{24}Mg^+/^{28}Si^+$/Fo content values represent differences in Mg/Si RSFs among olivine RMs. Although it may be logical to use molar Mg/Si ratio instead of Fo content for the normalization, calibrations using Fo content and molar Mg/Si ratio are very similar to each other. In addition, the Fo content of unknown olivine samples can be easily determined by electron microscopic techniques (e.g., SEM-EDS). Therefore, we use ($^{24}Mg^+/^{28}Si^+$/Fo) values instead of Mg/Si RSFs for the sake of convenience. In the case of O^- analysis (Fig. 8a), the bias*$_{25\ (RM\text{-}SCOl)}$ values of 15 olivine RMs with various Fo contents ranging from 59.3 to 97.4 are positively correlated with ($^{24}Mg^+/^{28}Si^+$/Fo) values and can be fitted with a quadratic function. However, two olivine RMs that are near-pure forsterite (SK-Ol and HN-Ol) do not follow the regression curve from other 15 olivine RMs. In the case of O_2^- analysis (Fig. 8b), the bias*$_{25\ (RM\text{-}SCOl)}$ values can be fitted into two separate quadratic curves for Fo contents ranging from 59.3 to 88.8 and 88.8 to 100, respectively. These calibration curves are much smoother than those against Fo contents, and this would improve the accuracy of SIMS Mg isotope analyses of unknown olivine samples. Fig. 8c and d show residual bias*$_{25\ (RM\text{-}SCOl)}$ values calculated from these calibration curves, which are plotted as a function of Fo content. In the case of O^- analysis (Fig. 8c), the residual bias*$_{25\ (RM\text{-}SCOl)}$ values are within ±0.4‰, except for two forsterite (SK-Ol and HN-Ol). In the case of O_2^- analysis (Fig. 8d), the residual bias*$_{25\ (RM\text{-}SCOl)}$ values of all olivine RMs are within ±0.2‰ that is smaller than analytical uncertainties (≤ ±0.3‰, 2σ). According the calibration scheme, precision and accuracy of bias*$_{25\ (RM\text{-}SCOl)}$ correction for O_2^- analysis would be 0.3‰ for olivine samples with $Fo_{59–100}$.

Note that the current suite of olivine RMs does not cover the range of Fo contents at around 87 and between 98 and 100, where both the bias*$_{25\ (RM\text{-}SCOl)}$ and ($^{24}Mg^+/^{28}Si^+$/Fo) change significantly within a small range of Fo content. Unknown analyses of olivine with these Fo contents may require additional RMs that match the minor element content of the unknown sample. Confirmation of consistent ionization

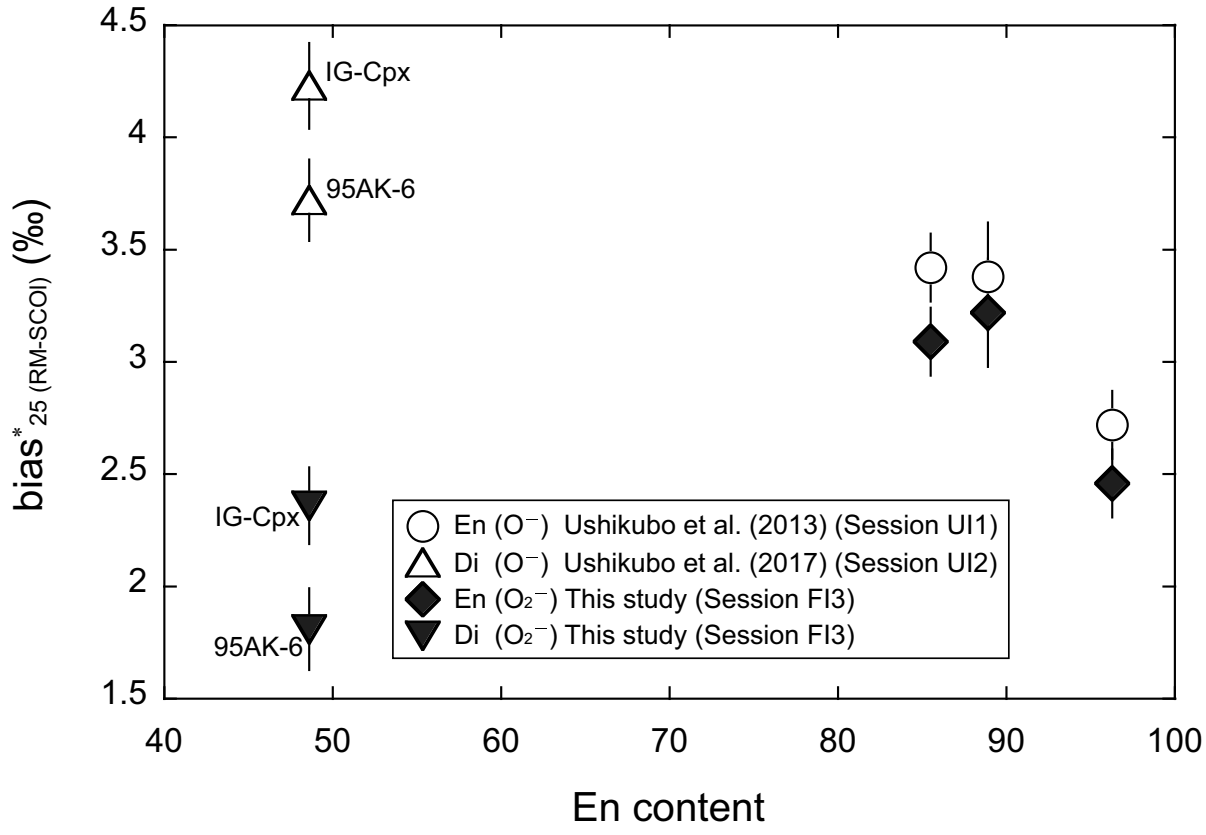

Fig. 6. The bias*$_{25\ (RM\text{-}SCOl)}$ values of 5 pyroxene RMs obtained by O^- and O_2^- analyses as a function of En content. Data for O^- analysis (open symbols) are from Ushikubo et al. (2013, 2017), which are re-normalized to the DSM-3 scale using the $\delta^{25}Mg_{DSM\text{-}3}$ values reported in this study. Errors are 2σ.

yields of Mg and Si between RM and unknown olivine with similar Fo content could be used to evaluate reliability of SIMS Mg isotope analyses. It should be noted that we combine the IMF and $^{24}Mg^+/^{28}Si^+$ ratios obtained with very different primary ion intensities (e.g., 1 nA and 6 pA for analyses with O_2^-), suggesting that these data are acquired from different depths. As mentioned above, the functionality of IMF against Fo content changes significantly with depth (Fig. 4), while relative $^{24}Mg^+/^{28}Si^+$ ratios do not (see Appendix EA7). As a result, the proposed calibration scheme would not work very well for Mg isotope analyses obtained from greater depths. This also means that the complex matrix effects in unknown olivine samples can be properly corrected only if a series of RMs are analyzed under the same analytical conditions, such as primary beam setting, integration time and cycle numbers, differences in which may change the depths of the analyses. The new RF plasma ion source maintains constant primary beam intensity (typically ±2%, 1SD) without changes in beam diameters in a week-long analysis session, in contrast to significant changes observed for a Duoplasmatron ion source (>30% in intensity and >50% in beam diameters; e.g., Tenner et al., 2019). Thus, the use of stable ion source, like RF plasma ion source, would be critical in obtaining more reliable SIMS Mg isotope analyses.

5.1.4. Instrumental bias of pyroxene

Five pyroxene RMs define a complex variation in IMF as a function of En content for O_2^- analysis (Fig. 6). Ushikubo et al. (2013, 2017) evaluated IMF on the same set of pyroxene RMs using an O^- primary ion beam, and assuming that the $\delta^{25,26}Mg_{DSM\text{-}3}$ values of these pyroxenes matched that of pyroxene from the Earth's mantle (−0.13 ± 0.04‰, 2SD; Teng et al., 2010). Here the bias*$_{25\ (RM\text{-}SCOl)}$ values reported in Ushikubo et al. (2013, 2017) are recalculated by using $\delta^{25}Mg_{DSM\text{-}3}$ values of each pyroxene RM obtained by SN-MC-ICP-MS analyses and these, along with the values determined using a O_2^- primary beam from this study are shown in Table 6 and Fig. 6. Ushikubo et al. (2013, 2017) also conducted multiple grain analyses of 5 pyroxene RMs so that we used the results as $\delta^{25}Mg$ homogeneities of each pyroxene RM to evaluate errors for bias*$_{25\ (RM\text{-}SCOl)}$ values. The original SIMS raw data obtained by Ushikubo et al. (2013, 2017) are shown in Appendix EA6. Homogeneities on $\delta^{25}Mg_m$ values of each pyroxene RM are summarized in Appendix EA4 and are within ±0.23‰ (2SD).

For the three orthopyroxene RMs (JE En, IG-Opx, and Sp79-11 En), bias*$_{25\ (RM\text{-}SCOl)}$ values obtained by O^- and O_2^- analyses are similar to each other (Fig. 6). However, the bias*$_{25\ (RM\text{-}SCOl)}$ values of two clinopyroxene RMs (IG-Cpx and 95AK-6 Di) differ by ~2‰ between O^- and O_2^- analyses. In both cases of O^- and O_2^- analyses, the bias*$_{25\ (RM\text{-}SCOl)}$ values of IG-Cpx are ~0.5‰ higher than that of 95AK-6 Di even though these clinopyroxenes have identical En content ($En_{48.6}$). Note that IG-Cpx contains Cr (Cr_2O_3 = 0.9 wt%), but 95AK-6 Di does not (Cr_2O_3 < 0.07 wt%). Moreover, the two clinopyroxene RMs differ in their Al_2O_3 contents (4.5 wt% in IG-Cpx and 0.9 wt% in 96AK-6 Di), implying that the instrumental bias on pyroxene may be sensitive to minor element abundances. However, because only 5 pyroxene RMs have been studied, further studies on a range of pyroxenes that differ in their En and Wo contents is needed to fully evaluate matrix effects on SIMS Mg isotope analysis of pyroxene.

5.2. Selection and preparation of olivine and pyroxene reference materials for SIMS Mg isotope analysis

In order to conduct SIMS analyses on olivine and pyroxene that are both accurate and precise it is a best practice to characterize the Mg isotope composition of the RM using either SN-MC-ICP-MS or fs-LA-MC-ICP-MS with water addition. However, for some materials such as olivine and pyroxene from terrestrial mantle-derived peridotites (e.g.,

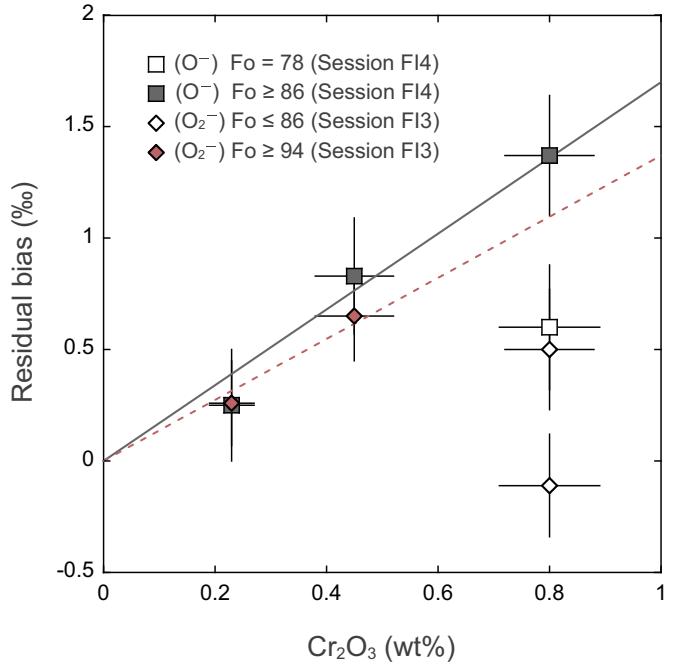

Fig. 7. Differences between bias*$_{25\ (RM\text{-}SCOl)}$ and modelled bias*$_{25\ (RM\text{-}SCOl)}$ values of Cr-bearing olivine RMs as a function of Cr_2O_3 content obtained by EPMA analyses. The modelled value (bias*$_{25\ (RM\text{-}SCOl)}$) is calculated by assuming linear correlation between bias*$_{25\ (RM\text{-}SCOl)}$ value and Fo content among olivine RMs with similar Fo contents (see Appendix EA8 for details). A solid and dashed lines represent least-squares regression lines for Cr-bearing olivine RMs with Fo ≥ 86 (O^- analysis) and that with Fo ≥ 94 (O_2^- analysis), respectively. Assuming intercepts with zero, the slopes are determined to be 1.7 ± 0.3 (2 σ, MSDW = 0.6) for O^- analysis and 1.4 ± 0.4 (2 σ, MSDW = 0.4) for O_2^- analysis, respectively. Errors of Cr_2O_3 (wt%) and residual bias are 2SD and 2σ, respectively.

mantle xenoliths) or igneous rocks one can assume the material has a mantle-like Mg isotope composition ($\delta^{25}Mg_{DSM\text{-}3}$ = −0.13 ± 0.04‰, 2SD; Teng et al., 2010). For example, four terrestrial olivine (SC-Ol, UWOL-1, IG-Ol, and HaK-Ol) and 2 pyroxene (IG-Opx and IG-Cpx) RMs were obtained from mantle-derived peridotites and these RMs have $\delta^{25}Mg_{DSM\text{-}3}$ that ranged from −0.14 ± 0.10 to −0.03 ± 0.09‰ (2SD). Moreover, a terrestrial olivine RM from a gabbro (FJ-Ol), a terrestrial olivine RM from a komatiite (WK-Ol), and a terrestrial orthopyroxene (Sp79-11 En) also have mantle-like $\delta^{25}Mg_{DSM\text{-}3}$ values ranging from −0.09 ± 0.13‰ to −0.06 ± 0.05‰ (2SD). Meteoritic samples also tend to have a limited range in Mg isotope compositions. Where, for example, chondrites have an average $\delta^{25}Mg_{DSM\text{-}3}$ = −0.15 ± 0.04‰ (2SD; Teng et al., 2010), and bulk achondrites overlap with the terrestrial mantle and chondritic Mg isotope ratios (Sedaghatpour and Teng, 2016). In our study, meteorite olivine RMs include samples from an ureilites (Kenna and ALH77257), a pallasite (Springwater), a winonaite (Winona), and an ungrouped achondrite (NWA 7325). These meteoritic olivine RMs have a limited variation in $\delta^{25}Mg_{DSM\text{-}3}$ values ranging from −0.07 ± 0.14 to 0.04 ± 0.17‰ (2SD) that are indistinguishable from the average $\delta^{25}Mg_{DSM\text{-}3}$ value of the Earth's mantle and chondrites.

Olivine and pyroxene RMs that were either synthetically produced or came from a metamorphosed carbonate have Mg isotope compositions that are significantly different as compared to terrestrial mantle or chondritic Mg isotope compositions. For these types of samples, one must determine their Mg isotope composition by either SN-MC-ICP-MS or fs-LA-MC-ICP-MS if they are to be used to conduct accurate and precise Mg isotope analysis by SIMS. The synthetic pure forsterite RM (HN-Ol), that is endmember Fo, has a $\delta^{25}Mg_{DSM\text{-}3}$ value −0.37 ± 0.09‰ (2SD) as determined by SN-MC-ICP-MS. This Mg isotope composition reflects the Mg isotope composition of the reagents used to synthesize the olivine, as well as any mass-dependent fractionation that occurred during its synthesis (e.g., Kita et al., 2012). Additionally, olivine and pyroxene RMs that were obtained from metamorphosed carbonate rocks have Mg isotope compositions that are significantly different than mantle or chondritic compositions. These differences arise because Mg-bearing carbonates have lower $\delta^{25}Mg_{DSM\text{-}3}$ values as compared to silicates (e.g., Young and Galy, 2004). These low $\delta^{25}Mg_{DSM\text{-}3}$ values reflect the fact that at equilibrium Mg-bearing carbonates have low $\delta^{25}Mg_{DSM\text{-}3}$ values by 2–3‰ relative to aqueous Mg at room temperature (Li et al., 2015). Moreover, Mg-bearing dolomite in hydrothermally altered rocks show $\delta^{25}Mg_{DSM\text{-}3}$ values ranging from −1.15 to −0.23‰ (e.g., Azmy et al., 2013; Lavoie et al., 2014; Geske et al., 2015). Two of the olivine RMs are from metamorphosed carbonates (SK-Ol and 95AK-6 Di) and these samples have distinct Mg isotope ratios compared to igneous rocks. SK-Ol is nearly pure forsterite ($Fo_{99.8}$) that came from a marble from the Beinn an Dubhaich aureole, Isle of Skye, Scotland, where the olivine was produced by the contact metamorphism of dolomite (e.g., Ferry et al., 2011). This olivine has the lowest $\delta^{25}Mg_{DSM\text{-}3}$ value (−0.89 ± 0.20‰, 2SD) of all the RMs considered in this study. Additionally, 95AK-6 Di is a clinopyroxene RM, that is from a marble, and this sample has the second lowest $\delta^{25}Mg_{DSM\text{-}3}$ value (−0.74 ± 0.05‰, 2SD).

5.3. Implications for Mg isotope fractionations of olivine in meteoritic components

In the WiscSIMS laboratory, 4 out of 17 olivine RMs (SC-Ol, HN-Ol, IG-Ol, and OR-Ol) have been used for instrumental bias corrections for Mg isotope analyses of olivine in Ca, Al-rich inclusions (CAIs), amoeboid olivine aggregates (AOAs), and chondrules (MacPherson et al., 2012, 2017; Ushikubo et al., 2013, 2017; Hertwig et al., 2019; Tenner et al., 2019). Although these previous analyses were conducted to determine the excess $\delta^{26}Mg^*$ after mass fractionation corrections, MacPherson et al. (2012, 2017) and Ushikubo et al. (2017) reported $\delta^{25}Mg$ values of olivine grains in CAIs and AOAs, which show large variations ranging from −2.8 to 11.3‰. The observed variations are much larger than the observed range of the instrumental bias on 17 olivine RMs in this study so that some extent of variations may exist in Mg isotope ratios of olivine among CAIs and AOAs. Furthermore, Ushikubo et al. (2013) reported $\delta^{25}Mg$ values of olivine grains in chondrules, which are systematically higher (up to 2.3‰) than those of coexisting phases (pyroxene and plagioclase). Based on the observations, Ushikubo et al. (2013) suggested that chondrule melting likely occurred in an open system process. However, these data were corrected for IMF using a calibration scheme based on the relationship between instrumental bias and Fo content (Fig. 2a), which fortuitously showed linear relationship if only these 4 RMs (SC-Ol, HN-Ol, IG-Ol, and OR-Ol) were utilized. The IMF of these 4 RMs that were obtained by using the Duoplasmatron source (Ushikubo et al., 2013) are consistent with our results that are obtained by using the RF plasma ion source (Fig. 2a), suggesting that the complex IMF observed in this study is not due to the difference in the primary ion sources (i.e., Duoplasmatron versus RF plasma). Moreover, as noted in Section 5.1.2, Cr-bearing olivine RMs (up to 0.8 wt% in Cr_2O_3) tend to show larger bias*$_{25\ (RM\text{-}SCOl)}$ values relative to those of olivine RMs with similar Fo contents (Fig. 7), which were not included for the calibration during the analysis session (Fig. 2a). Olivine grains in chondrules measured by Ushikubo et al. (2013) typically have substantial amount of Cr (up to 1.1 wt% in Cr_2O_3) so that at least a part of the observed Mg isotope variability identified in chondrule olivine may be an analytical artifacts caused by matrix effects. Note that the simple linear regression between IMF and Fo content as done by Ushikubo et al. (2013) may induce additional uncertainties on the IMF correction even if Cr-bearing RMs are not considered for the regression. Further studies based on a suitable set of standards and new calibration scheme based on the combination of

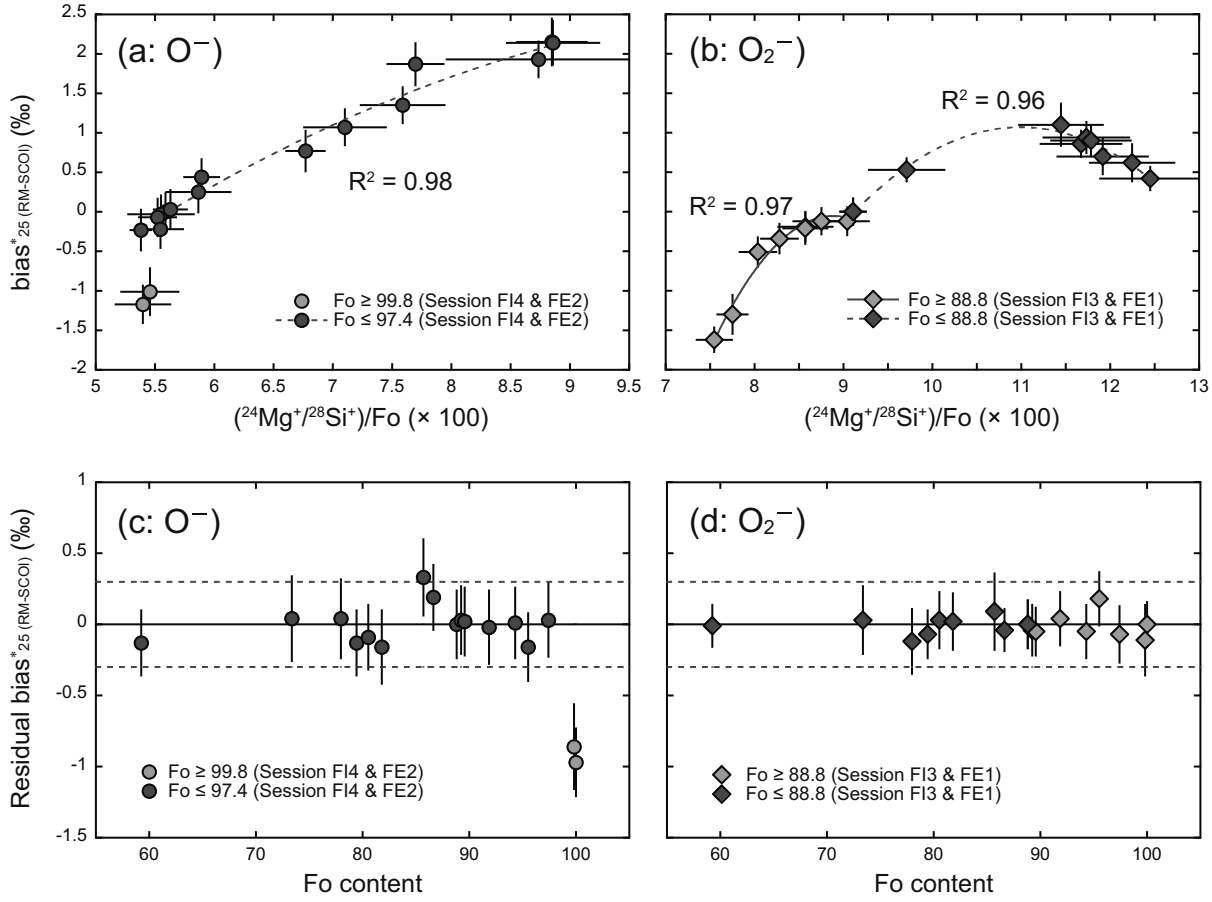

Fig. 8. The relationships between bias*$_{25\ (RM\text{-}SCOl)}$ values and $^{24}Mg^+/^{28}Si^+$ ratios divided by Fo contents of 17 olivine RMs. (a) In the case of O^- analysis, the bias*$_{25\ (RM\text{-}SCOl)}$ values of 15 olivine RMs with $Fo_{59.3}$ to $Fo_{97.4}$ are positively correlated with ($^{24}Mg^+/^{28}Si^+$/Fo) values. The dashed curve represents a quadratic function regression curve (bias*$_{25\ (RM\text{-}SCOl)} = -0.08 \times (^{24}Mg^+/^{28}Si^+/Fo)^2 + 1.76 \times (^{24}Mg^+/^{28}Si^+/Fo) - 7.48$; $R^2 = 0.98$). Note that two nearly pure forsterite RMs (SK-Ol and HN-Ol) do not follow the regression curve. (b) In the case of O_2^- analysis, the bias*$_{25\ (RM\text{-}SCOl)}$ values can be fitted into two separate quadratic curves for Fo contents ranging from 59.3 to 88.8 and 88.8 to 100, respectively. The dashed curve represents the quadratic function regression curve for Fo content ≤ 88.8 (bias*$_{25\ (RM\text{-}SCOl)} = -0.31 \times (^{24}Mg^+/^{28}Si^+/Fo)^2 + 6.77 \times (^{24}Mg^+/^{28}Si^+/Fo) - 36.14$; $R^2 = 0.96$) and the solid curve represents the quadratic function regression curve for Fo content ≥ 88.8 (bias*$_{25\ (RM\text{-}SCOl)} = -0.87 \times (^{24}Mg^+/^{28}Si^+/Fo)^2 + 15.43 \times (^{24}Mg^+/^{28}Si^+/Fo) - 68.67$; $R^2 = 0.97$). (c, d) Plots of the calibration residuals as a function of Fo content for O^- and O_2^- analyses, respectively. For O_2^- analysis, bias*$_{25\ (RM\text{-}SCOl)}$ values of all RMs differs by <0.3‰ (depicted by dashed lines) from the value predicted by the calibration (solid line). Errors are 2σ.

Mg^+/Si^+ ratios and Fo contents is required to more accurately determine Mg isotope compositions in chondrule olivine grains. Accurate Mg isotope data that is free of matrix effects will allow one to better address if chondrules formed in an open system in the protoplanetary disk.

6. Conclusion

We performed Mg isotope analyses of 17 olivine and 5 pyroxene RMs using MC-ICP-MS and MC-SIMS and evaluated SIMS matrix effects on Mg isotope analysis.

(1) No significant matrix effects on fs-LA-MC-ICP-MS analysis of olivine ($Fo_{59.3}$ to Fo_{100}) within analytical uncertainties (≤0.2‰ in $\delta^{25}Mg$, 2SD) under the wet plasma condition (a rate of introducing water = 40 μL/min).
(2) The IMF for SIMS Mg isotope analysis of olivine ($Fo_{59.3}$ to Fo_{100}) ranges over ~3.3‰ in $\delta^{25}Mg$ and is a complex function of Fo content. Moreover, the inferred IMF changes by ~2.9‰ in $\delta^{25}Mg$ during a long duration (50 min) spot analysis, suggesting that the IMF of an olivine analysis may change as a function of the depth of the analysis.
(3) For olivine analyses, the relationship between variations in the Mg/Si RSF and IMF, as a function of olivine Fo content, are similar suggesting that the instrumental mass bias changes in part because of differences in the ionization efficiency of Mg and Si. Minor element abundances (e.g., Cr) may also influence secondary ionization processes, especially for Mg-rich olivine. This minor element variability may be the cause of the complex behavior of the IMF as a function of Fo content for the high Fo olivine RMs.
(4) The instrumental bias among most olivine RMs can be fitted using a quadratic function relative to the sensitivity of Mg and Si ions, expressed as ($^{24}Mg^+/^{28}Si^+$/Fo). According to the regression curve, precision and accuracy of bias*$_{25\ (RM\text{-}SCOl)}$ correction would be 0.3‰ for O_2^- analysis.
(5) The magnitudes of IMF on SIMS Mg isotope analysis of pyroxene ($En_{48.6}$ to $En_{96.3}$) range over ~1.4‰ in $\delta^{25}Mg$, which is approximately one half the range as measured in olivine over a similar range in Fe/Mg variation. The Mg isotope IMF on pyroxene is not a smooth function of En content, indicating that additional factors (e.g., minor element abundances) may influence matrix effects. Further studies are required for accurate SIMS Mg isotope analysis of pyroxene.
(6) Most olivine and pyroxene RMs from igneous rocks do not show significant variations in $\delta^{25}Mg_{DSM\text{-}3}$ values (≤0.3‰). Therefore, $\delta^{25}Mg_{DSM\text{-}3}$ values of these samples may be assumed to have the

same value of the Earth's mantle (−0.13‰: Teng et al., 2010) and such samples can be used as RMs for SIMS Mg isotope analysis. In contrast, $\delta^{25}Mg_{DSM\text{-}3}$ values of RMs from olivine and pyroxene derived from metamorphosed carbonate rocks have $\delta^{25}Mg_{DSM\text{-}3}$ values that are ~1‰ lower than that of the Earth's mantle. Synthetic olivine and pyroxene are also likely to have $\delta^{25}Mg_{DSM\text{-}3}$ values that do not match the terrestrial mantle and for these samples the $\delta^{25}Mg_{DSM\text{-}3}$ values of these RMs must be determined by independent methods such as SN-MC-ICP-MS or fs-LA-MC-ICP-MS.

Supplementary data to this article can be found online at https://doi.org/10.1016/j.chemgeo.2020.119482.

Declaration of competing interest

The authors declare that they have no known competing financial interests or personal relationships that could have appeared to influence the work reported in this paper.

Acknowledgements

We are grateful to Kouki Kitajima for his valuable comments and developments of SIMS operation and data reduction procedures. We thank Timothy McCoy and Julie Hoskin (Smithsonian Institution) for allocating Winona, Kenna, and Springwater meteorites for the study. We thank Katsuyuki Yamashita, Cyrena Goodrich, Alexander Sobolev, Shichun Huang, and Fang-Zhen Teng for generously providing meteorite and rock samples (ALH77257, NWA 7325, Weltevreden komatiite, and CL09 series). Several WiscSIMS oxygen standards used in this work were provided by John Valley. We thank Guillaume Siron for assistance with electron microprobe analyses. We are grateful to Steve Romaniello and Rebekah Hines for their invaluable assistance in the IGCL at ASU. We also thank Kazuhide Nagashima and an anonymous reviewer for constructive comments that improved the quality of the paper and Balz Kamber for prompt editorial handling of this paper. This work is supported by the NASA program (NNX16AG80G to NK and NNX15AH41G to MW). WiscSIMS is partly supported by NSF (EAR 1658823).

References

Albarède, F., Beard, B., 2004. Analytical methods for non-traditional isotopes. Rev. Mineral. Geochemistry 55, 113–152.
Albarède, F., Telouk, P., Blichert-Toft, J., Boyet, M., Agranier, A., Nelson, B., 2004. Precise and accurate isotopic measurements using multiple-collector ICPMS. Geochim. Cosmochim. Acta 68, 2725–2744.
Azmy, K., Lavoie, D., Wang, Z., Brand, U., Al-Aasm, I., Jackson, S., Girard, I., 2013. Magnesium-isotope and REE compositions of Lower Ordovician carbonates from eastern Laurentia: implications for the origin of dolomites and limestones. Chem. Geol. 356, 64–75.
Bourdon, B., Tipper, E.T., Fitoussi, C., Stracke, A., 2010. Chondritic Mg isotope composition of the earth. Geochim. Cosmochim. Acta 74, 5069–5083.
Bouvier, A., Spivak-Birndorf, L.J., Brennecka, G.A., Wadhwa, M., 2011. New constraints on early solar system chronology from Al-Mg and U-Pb isotope systematics in the unique basaltic achondrite Northwest Africa 2976. Geochim. Cosmochim. Acta 75, 5310–5323.
Bullock, E.S., Knight, K.B., Richter, F.M., Kita, N.T., Ushikubo, T., MacPherson, G.J., Davis, A.M., Mendybaev, R.A., 2013. Mg and Si isotopic fractionation patterns in types B1 and B2 CAIs: implications for formation under different nebular conditions. Meteorit. Planet. Sci. 48, 1440–1458.
Catanzaro, E.J., Murphy, T.J., Garner, E.L., Shields, W.R., 1966. Absolute isotopic abundance ratios and atomic weight of magnesium. J. Res. Natl. Bur. Stand. Sect. A Phys. Chem. 70A, 453–458.
Chaussidon, M., Deng, Z., Watson, B., Richter, F., 2017. In situ analysis of non-traditional isotopes by SIMS and LA–MC–ICP–MS: key aspects and the example of Mg isotopes in olivines and silicate glasses. Rev. Mineral. Geochemistry 82, 127–163.
Davis, A.M., Richter, F.M., Mendybaev, R.A., Janney, P.E., Wadhwa, M., McKeegan, K.D., 2015. Isotopic mass fractionation laws for magnesium and their effects on ^{26}Al–^{26}Mg systematics in solar system materials. Geochim. Cosmochim. Acta 158, 245–261.
Donovan, J.J., Tingle, T.N., 1996. An improved mean atomic number background correction for quantitative microanalysis. Microsc. Microanal. 2, 1–7.
Eiler, J.M., Graham, C., Valley, J.W., 1997. SIMS analysis of oxygen isotopes: matrix effects in complex minerals and glasses. Chem. Geol. 138, 221–244.
Ferry, J.M., Ushikubo, T., Valley, A.W., 2011. Formation of forsterite by silicification of dolomite during contact metamorphism. J. Petrol. 52, 1619–1640.
Galy, A., Belshaw, N.S., Halicz, L., O'Nions, R.K., 2001. High-precision measurement of magnesium isotopes by multiple-collector inductively coupled plasma mass spectrometry. Int. J. Mass Spectrom. 208, 89–98.
Galy, A., Yoffe, O., Janney, P.E., Williams, R.W., Cloquet, C., Alard, O., Halicz, L., Wadhwa, M., Hutcheon, I.D., Ramon, E., Carignan, J., 2003. Magnesium isotope heterogeneity of the isotopic standard SRM980 and new reference materials for magnesium-isotope-ratio measurements. J. Anal. At. Spectrom. 18, 1352.
Geske, A., Goldstein, R.H., Mavromatis, V., Richter, D.K., Buhl, D., Kluge, T., John, C.M., Immenhauser, A., 2015. The magnesium isotope ($\delta^{26}Mg$) signature of dolomites. Geochim. Cosmochim. Acta 149, 131–151.
Goodrich, C.A., Kita, N.T., Yin, Q.Z., Sanborn, M.E., Williams, C.D., Nakashima, D., Lane, M.D., Boyle, S., 2017. Petrogenesis and provenance of ungrouped achondrite Northwest Africa 7325 from petrology, trace elements, oxygen, chromium and titanium isotopes, and mid-IR spectroscopy. Geochim. Cosmochim. Acta 203, 381–403.
Handler, M.R., Baker, J.A., Schiller, M., Bennett, V.C., Yaxley, G.M., 2009. Magnesium stable isotope composition of earth's upper mantle. Earth Planet. Sci. Lett. 282, 306–313.
Hertwig, A.T., Kimura, M., Ushikubo, T., Defouilloy, C., Kita, N.T., 2019. The ^{26}Al–^{26}Mg systematics of FeO-rich chondrules from Acfer 094: two chondrule generations distinct in age and oxygen isotope ratios. Geochim. Cosmochim. Acta 253, 111–126.
Horn, I., von Blanckenburg, F., 2007. Investigation on elemental and isotopic fractionation during 196 nm femtosecond laser ablation multiple collector inductively coupled plasma mass spectrometry. Spectrochim. Acta - Part B At. Spectrosc. 62, 410–422.
Hu, Y., Teng, F.Z., Zhang, H.F., Xiao, Y., Su, B.X., 2016a. Metasomatism-induced mantle magnesium isotopic heterogeneity: evidence from pyroxenites. Geochim. Cosmochim. Acta 185, 88–111.
Hu, Y., Harrington, M.D., Sun, Y., Yang, Z., Konter, J., Teng, F.Z., 2016b. Magnesium isotopic homogeneity of San Carlos olivine: a potential standard for Mg isotopic analysis by multi-collector inductively coupled plasma mass spectrometry. Rapid Commun. Mass Spectrom. 2123–2132.
Isa, J., Kohl, I.E., Liu, M.C., Wasson, J.T., Young, E.D., McKeegan, K.D., 2017. Quantification of oxygen isotope SIMS matrix effects in olivine samples: correlation with sputter rate. Chem. Geol. 458, 14–21.
Jacobsen, B., Yin, Q. zhu, Moynier, F., Amelin, Y., Krot, A.N., Nagashima, K., Hutcheon, I.D., Palme, H., 2008. ^{26}Al–^{26}Mg and ^{207}Pb–^{206}Pb systematics of Allende CAIs: canonical solar initial $^{26}Al/^{27}Al$ ratio reinstated. Earth Planet. Sci. Lett. 272, 353–364.
Kawasaki, N., Kato, C., Itoh, S., Wakaki, S., Ito, M., Yurimoto, H., 2015. ^{26}Al-^{26}Mg chronology and oxygen isotope distributions of multiple melting for a Type C CAI from Allende. Geochim. Cosmochim. Acta 169, 99–114.
Kawasaki, N., Itoh, S., Sakamoto, N., Yurimoto, H., 2017. Chronological study of oxygen isotope composition for the solar protoplanetary disk recorded in a fluffy Type A CAI from Vigarano. Geochim. Cosmochim. Acta 201, 83–102.
Kawasaki, N., Simon, S.B., Grossman, L., Sakamoto, N., Yurimoto, H., 2018. Crystal growth and disequilibrium distribution of oxygen isotopes in an igneous Ca-Al-rich inclusion from the Allende carbonaceous chondrite. Geochim. Cosmochim. Acta 221, 318–341.
Kawasaki, N., Park, C., Sakamoto, N., Park, S.Y., Kim, H.N., Kuroda, M., Yurimoto, H., 2019. Variations in initial $^{26}Al/^{27}Al$ ratios among fluffy Type A Ca–Al-rich inclusions from reduced CV chondrites. Earth Planet. Sci. Lett. 511, 25–35.
Kita, N.T., Nagahara, H., Togashi, S., Morishita, Y., 2000. A short duration of chondrule formation in the solar nebula: evidence from ^{26}Al in Semarkona ferromagnesian chondrules. Geochim. Cosmochim. Acta 64, 3913–3922.
Kita, N.T., Ushikubo, T., Fu, B., Valley, J.W., 2009. High precision SIMS oxygen isotope analysis and the effect of sample topography. Chem. Geol. 264, 43–57.
Kita, N.T., Nagahara, H., Tachibana, S., Tomomura, S., Spicuzza, M.J., Fournelle, J.H., Valley, J.W., 2010. High precision SIMS oxygen three isotope study of chondrules in LL3 chondrites: Role of ambient gas during chondrule formation. Geochim. Cosmochim. Acta 74, 6610–6635.
Kita, N.T., Ushikubo, T., Knight, K.B., Mendybaev, R.A., Davis, A.M., Richter, F.M., Fournelle, J.H., 2012. Internal ^{26}Al–^{26}Mg isotope systematics of a Type B CAI: remelting of refractory precursor solids. Geochim. Cosmochim. Acta 86, 37–51.
Koefoed, P., Amelin, Y., Yin, Q.Z., Wimpenny, J., Sanborn, M.E., Iizuka, T., Irving, A.J., 2016. U–Pb and Al–Mg systematics of the ungrouped achondrite Northwest Africa 7325. Geochim. Cosmochim. Acta 183, 31–45.
Krot, A.N., Nagashima, K., Wasserburg, G.J., Huss, G.R., Papanastassiou, D., Davis, A.M., Hutcheon, I.D., Bizzarro, M., 2014. Calcium-aluminum-rich inclusions with fractionation and unknown nuclear effects (FUN CAIs): I. Mineralogy, petrology, and oxygen isotopic compositions. Geochim. Cosmochim. Acta 145, 206–247.
Larsen, K.K., Trinquier, A., Paton, C., Schiller, M., Wielandt, D., Ivanova, M.A., Connelly, J.N., Nordlund, Å., Krot, A.N., Bizzarro, M., 2011. Evidence for magnesium isotope heterogeneity in the solar protoplanetary disk. Astrophys. J. Lett. 735.
Lavoie, D., Jackson, S., Girard, I., 2014. Magnesium isotopes in high-temperature saddle dolomite cements in the lower Paleozoic of Canada. Sediment. Geol. 305, 58–68.
Li, W., Beard, B.L., Li, C., Xu, H., Johnson, C.M., 2015. Experimental calibration of Mg isotope fractionation between dolomite and aqueous solution and its geological implications. Geochim. Cosmochim. Acta 157, 164–181.
Luu, T.-H., Chaussidon, M., Mishra, R.K., Rollion-Bard, C., Villeneuve, J., Srinivasan, G., Birck, J.-L., 2013. High precision Mg isotope measurements of meteoritic samples by secondary ion mass spectrometry. J. Anal. At. Spectrom. 28, 67–76.
MacPherson, G.J., Kita, N.T., Ushikubo, T., Bullock, E.S., Davis, A.M., 2012. Well-resolved variations in the formation ages for Ca-Al-rich inclusions in the early Solar System. Earth Planet. Sci. Lett. 331–332, 43–54.
MacPherson, G.J., Bullock, E.S., Tenner, T.J., Nakashima, D., Kita, N.T., Ivanova, M.A., Krot, A.N., Petaev, M.I., Jacobsen, S.B., 2017. High precision Al–Mg systematics of

forsterite-bearing Type B CAIs from CV3 chondrites. Geochim. Cosmochim. Acta 201, 65–82.
Mendybaev, R.A., Richter, F.M., Georg, R.B., Janney, P.E., Spicuzza, M.J., Davis, A.M., Valley, J.W., 2013. Experimental evaporation of Mg- and Si-rich melts: implications for the origin and evolution of FUN CAIs. Geochim. Cosmochim. Acta 123, 368–384.
Mendybaev, R.A., Williams, C.D., Spicuzza, M.J., Richter, F.M., Valley, J.W., Fedkin, A.V., Wadhwa, M., 2017. Thermal and chemical evolution in the early Solar System as recorded by FUN CAIs: part II – laboratory evaporation of potential CMS-1 precursor material. Geochim. Cosmochim. Acta 201, 49–64.
Oeser, M., Weyer, S., Horn, I., Schuth, S., 2014. High-precision fe and mg isotope ratios of silicate reference glasses determined in situ by femtosecond LA-MC-ICP-MS and by solution nebulisation MC-ICP-MS. Geostand. Geoanalytical Res. 38, 311–328.
Olsen, M.B., Wielandt, D., Schiller, M., Van Kooten, E.M.M.E., Bizzarro, M., 2016. Magnesium and ^{54}Cr isotope compositions of carbonaceous chondrite chondrules – insights into early disk processes. Geochim. Cosmochim. Acta 191, 118–138.
Park, C., Nagashima, K., Krot, A.N., Huss, G.R., Davis, A.M., Bizzarro, M., 2017. Calcium-aluminum-rich inclusions with fractionation and unidentified nuclear effects (FUN CAIs): II. Heterogeneities of magnesium isotopes and ^{26}Al in the early solar system inferred from in situ high-precision magnesium-isotope measurements. Geochim. Cosmochim. Acta 201, 6–24.
Peres, P., Kita, N.T., Valley, J.W., Fernandes, F., Schuhmacher, M., 2013. New sample holder geometry for high precision isotope analyses. Surf. Interface Anal. 45, 553–556.
Pogge von Strandmann, P.A.E., Burton, K.W., James, R.H., van Calsteren, P., Gislason, S.R., Sigfússon, B., 2008. The influence of weathering processes on riverine magnesium isotopes in a basaltic terrain. Earth Planet. Sci. Lett. 276, 187–197.
Richter, F.M., Janney, P.E., Mendybaev, R.A., Davis, A.M., Wadhwa, M., 2007. Elemental and isotopic fractionation of Type B CAI-like liquids by evaporation. Geochim. Cosmochim. Acta 71, 5544–5564.
Schiller, M., Handler, M.R., Baker, J.A., 2010. High-precision Mg isotopic systematics of bulk chondrites. Earth Planet. Sci. Lett. 297, 165–173.
Scicchitano, M.R., Rubatto, D., Hermann, J., Majumdar, A.S., Putnis, A., 2018. Oxygen isotope analysis of olivine by ion microprobe: matrix effects and applications to a serpentinised dunite. Chem. Geol. 499, 126–137.
Sedaghatpour, F., Teng, F.Z., 2016. Magnesium isotopic composition of achondrites. Geochim. Cosmochim. Acta 174, 167–179.
Śliwiński, M.G., Kitajima, K., Kozdon, R., Spicuzza, M.J., Fournelle, J.H., Denny, A., Valley, J.W., 2016Aa. Secondary ion mass spectrometry bias on isotope ratios in dolomite–ankerite, part I: δ^{18}O matrix effects. Geostand. Geoanalytical Res. 40, 157–172.
Śliwiński, M.G., Kitajima, K., Kozdon, R., Spicuzza, M.J., Fournelle, J.H., Denny, A., Valley, J.W., 2016Ab. Secondary ion mass spectrometry bias on isotope ratios in dolomite–ankerite, part II: δ^{13}C matrix effects. Geostand. Geoanalytical Res. 40, 173–184.
Śliwiński, M.G., Kitajima, K., Spicuzza, M.J., Orland, I.J., Ishida, A., Fournelle, J.H., Valley, J.W., 2018. SIMS bias on isotope ratios in Ca-Mg-Fe carbonates (part III): δ^{18}O and δ^{13}C matrix effects along the magnesite–siderite solid-solution series. Geostand. Geoanalytical Res. 42, 49–76.
Spivak-Birndorf, L., Wadhwa, M., Janney, P., 2009. ^{26}Al–^{26}Mg systematics in D'Orbigny and Sahara 99555 angrites: Implications for high-resolution chronology using extinct chronometers. Geochim. Cosmochim. Acta 73, 5202–5211.
Steele, I.M., Hervig, R.L., Hutcheon, I.D., Smith, J.V., 1981. Ion microprobe techniques and analyses of olivine and low-Ca pyroxene. Am. Mineral. 66, 526–546.
Steinhoefel, G., Horn, I., von Blanckenburg, F., 2009. Matrix-independent Fe isotope ratio determination in silicates using UV femtosecond laser ablation. Chem. Geol. 268, 67–73.
Teng, F.Z., 2017. Magnesium isotope geochemistry. Rev. Mineral. Geochemistry 82, 219–287.
Teng, F.Z., Li, W.Y., Ke, S., Marty, B., Dauphas, N., Huang, S., Wu, F.Y., Pourmand, A., 2010. Magnesium isotopic composition of the earth and chondrites. Geochim. Cosmochim. Acta 74, 4150–4166.
Tenner, T.J., Nakashima, D., Ushikubo, T., Tomioka, N., Kimura, M., Weisberg, M.K., Kita, N.T., 2019. Extended chondrule formation intervals in distinct physicochemical environments: evidence from Al–Mg isotope systematics of CR chondrite chondrules with unaltered plagioclase. Geochim. Cosmochim. Acta 260, 133–160.
Tipper, E.T., Galy, A., Bickle, M.J., 2006. Riverine evidence for a fractionated reservoir of Ca and Mg on the continents: implications for the oceanic Ca cycle. Earth Planet. Sci. Lett. 247, 267–279.
Ushikubo, T., Nakashima, D., Kimura, M., Tenner, T.J., Kita, N.T., 2013. Contemporaneous formation of chondrules in distinct oxygen isotope reservoirs. Geochim. Cosmochim. Acta 109, 280–295.
Ushikubo, T., Tenner, T.J., Hiyagon, H., Kita, N.T., 2017. A long duration of the ^{16}O-rich reservoir in the solar nebula, as recorded in fine-grained refractory inclusions from the least metamorphosed carbonaceous chondrites. Geochim. Cosmochim. Acta 201, 103–122.
Valley, J.W., Kita, N.T., 2009. In situ oxygen isotope geochemistry by ion microprobe. In: Mineral. Assoc. Canada Short Course, pp. 19–63.
Van Kooten, E.M.M.E., Wielandt, D., Schiller, M., Nagashima, K., Thomen, A., Larsen, K.K., Olsen, M.B., Nordlund, Å., Krot, A.N., Bizzarro, M., 2016. Isotopic evidence for primordial molecular cloud material in metal-rich carbonaceous chondrites. Proc. Natl. Acad. Sci. 113, 2011–2016.
Villeneuve, J., Chaussidon, M., Marrocchi, Y., Deng, Z., Watson, E.B., 2019. High-precision in situ silicon isotopic analyses by MC-SIMS in olivine and low-Ca pyroxene. Rapid Commun. Mass Spectrom. 33, 1589–1597.
Wasserburg, G.J., Wimpenny, J., Yin, Q.Z., 2012. Mg isotopic heterogeneity, Al–Mg isochrons, and canonical ^{26}Al/^{27}Al in the early solar system. Meteorit. Planet. Sci. 47, 1980–1997.
Williams, C.D., Ushikubo, T., Bullock, E.S., Janney, P.E., Hines, R.R., Kita, N.T., Hervig, R.L., MacPherson, G.J., Mendybaev, R.A., Richter, F.M., Wadhwa, M., 2017. Thermal and chemical evolution in the early solar system as recorded by FUN CAIs: part I – petrology, mineral chemistry, and isotopic composition of Allende FUN CAI CMS-1. Geochim. Cosmochim. Acta 201, 25–48.
Xiao, Y., Teng, F.Z., Zhang, H.F., Yang, W., 2013. Large magnesium isotope fractionation in peridotite xenoliths from eastern North China craton: product of melt-rock interaction. Geochim. Cosmochim. Acta 115, 241–261.
Young, E.D., Galy, A., 2004. The isotope geochemistry and cosmochemistry of magnesium. Rev. Mineral. Geochemistry 55, 197–230.
Young, E.D., Ash, R.D., Galy, A., Belshaw, N.S., 2002. Mg isotope heterogeneity in the Allende meteorite measured by UV laser ablation-MC-ICPMS and comparisons with O isotopes. Geochim. Cosmochim. Acta 66, 683–698.
Zheng, X.Y., Beard, B.L., Johnson, C.M., 2018. Assessment of matrix effects associated with Fe isotope analysis using 266 nm femtosecond and 193 nm nanosecond laser ablation multi-collector inductively coupled plasma mass spectrometry. J. Anal. At. Spectrom. 33, 68–83.